


BRAIN COMMUNICATIONS

Cyclase-associated protein 2 dimerization regulates cofilin in synaptic plasticity and Alzheimer's disease

Silvia Pelucchi,^{1,2,*} Lina Vandermeulen,^{1,*}  Lara Pizzamiglio,³  Bahar Aksan,⁴ Jing Yan,⁴ Anja Konietzny,⁵ Elisa Bonomi,⁶ Barbara Borroni,⁶ Alessandro Padovani,⁶  Marco B. Rust,^{7,8,9} Daniele Di Marino,¹⁰ Marina Mikhaylova,^{5,11}  Daniela Mauceri,⁴ Flavia Antonucci,³  Valeria Edefonti,¹² Fabrizio Gardoni,¹ Monica Di Luca^{1,†} and Elena Marcello^{1,†}

*These authors are the co-first authors.

†These authors are the co-senior authors.

Regulation of actin cytoskeleton dynamics in dendritic spines is crucial for learning and memory formation. Hence, defects in the actin cytoskeleton pathways are a biological trait of several brain diseases, including Alzheimer's disease. Here, we describe a novel synaptic mechanism governed by the cyclase-associated protein 2, which is required for structural plasticity phenomena and completely disrupted in Alzheimer's disease. We report that the formation of cyclase-associated protein 2 dimers through its Cys³² is important for cyclase-associated protein 2 binding to cofilin and for actin turnover. The Cys³²-dependent cyclase-associated protein 2 homodimerization and association to cofilin are triggered by long-term potentiation and are required for long-term potentiation-induced cofilin translocation into spines, spine remodelling and the potentiation of synaptic transmission. This mechanism is specifically affected in the hippocampus, but not in the superior frontal gyrus, of both Alzheimer's disease patients and APP/PS1 mice, where cyclase-associated protein 2 is down-regulated and cyclase-associated protein 2 dimer synaptic levels are reduced. Notably, cyclase-associated protein 2 levels in the cerebrospinal fluid are significantly increased in Alzheimer's disease patients but not in subjects affected by frontotemporal dementia. In Alzheimer's disease hippocampi, cofilin association to cyclase-associated protein 2 dimer/monomer is altered and cofilin is aberrantly localized in spines. Taken together, these results provide novel insights into structural plasticity mechanisms that are defective in Alzheimer's disease.

- 1 Department of Pharmacological and Biomolecular Sciences, Università degli Studi di Milano, Milan, Italy
- 2 Department of Neurosciences, Psychology, Drug Research, and Child Health, University of Florence, Florence, Italy
- 3 Department of Biotechnology and Translational Medicine, Università degli Studi di Milano, Milan, Italy
- 4 Department of Neurobiology, Interdisciplinary Centre for Neurosciences (IZN), Heidelberg University, INF 366 69120, Heidelberg, Germany
- 5 Emmy-Noether Group "Neuronal Protein Transport", Center for Molecular Neurobiology Hamburg (ZMNH), University Medical Center Hamburg-Eppendorf (UKE), Falkenried 94, 20251, Hamburg, Germany
- 6 Neurology Unit, Centre for Neurodegenerative Disorders, Department of Clinical and Experimental Sciences, University of Brescia, Brescia, Italy
- 7 Faculty of Medicine, Molecular Neurobiology Group, Institute of Physiological Chemistry, University of Marburg, Marburg, Germany
- 8 DFG Research Training Group, Membrane Plasticity in Tissue Development and Remodeling, GRK 2213, Philipps-University of Marburg, 35032, Marburg, Germany

Received January 24, 2020. Revised April 24, 2020. Accepted April 28, 2020. Advance Access publication June 26, 2020

© The Author(s) (2020). Published by Oxford University Press on behalf of the Guarantors of Brain.

This is an Open Access article distributed under the terms of the Creative Commons Attribution Non-Commercial License (<http://creativecommons.org/licenses/by-nc/4.0/>), which permits non-commercial re-use, distribution, and reproduction in any medium, provided the original work is properly cited. For commercial re-use, please contact journals.permissions@oup.com

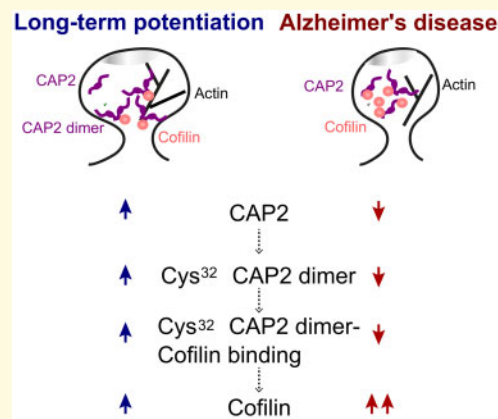
- 9 Center for Mind, Brain and Behavior (CMBB), University of Marburg and Justus-Liebig-University Giessen, Hans-Meerwein-Strasse 6, 35032, Marburg, Germany
- 10 Department of Life and Environmental Sciences, New York-Marche Structural Biology Center (NY-MaSBiC), Polytechnic University of Marche, Via Brecce Bianche, Ancona, Italy
- 11 Research Group “Optobiology”, Institute for Biology, Humboldt-Universität zu Berlin, Invalidenstraße 42, 10115 Berlin, Germany
- 12 Department of Clinical Sciences and Community Health, Branch of Medical Statistics, Biometry, and Epidemiology “G.A. Maccacaro”, Università degli Studi di Milano, Milan, Italy

Correspondence to: Monica Di Luca, Department of Pharmacological and Biomolecular Sciences, Università degli Studi di Milano, via Balzaretti 9, 20133 Milan, Italy
E-mail: monica.diluca@unimi.it

Keywords: dementia, synapse, actin, cytoskeleton

Abbreviations: AMPA = α -amino-3-hydroxy-5-methyl-4-isoxazolepropionic acid; CAP2 = cyclase-associated protein 2; CSF = cerebrospinal fluid; F-actin = filamentous actin; G-actin = globular actin; HC = healthy controls; LTD = long-term depression; LTP = long-term potentiation; PLA = proximity ligation assay; PSD-95 = postsynaptic density protein 95; PSD = postsynaptic densities; rAAV = recombinant adeno-associated virus; SFG = superior frontal gyrus; shr = shRNA-resistant; shRNA = small hairpin RNA; SIM = structured illumination microscopy; SS = synaptic stimulation; TIF = triton-insoluble fraction; WB = western blot; WT = wild-type

Graphical Abstract



Introduction

Dendritic spines are small dendritic protrusions containing excitatory postsynaptic machinery (Bourne and Harris, 2008). Since changes in spine morphology account for functional differences at the synaptic level (Yuste and Bonhoeffer, 2001), spine remodelling and modifications in spine density are believed to be important for learning and memory (Holtmaat and Svoboda, 2009) and are thereby associated with brain diseases characterized by cognitive decline, including Alzheimer's Disease (Penzes *et al.*, 2011). Indeed, it is widely accepted that spines constitute the anatomical locus of plasticity, where short-term alterations in synaptic strength are converted into long-lasting changes that are embedded in stable structural modifications (Sala and Segal, 2014). Hence, spine structural plasticity is tightly coordinated with synaptic function and plasticity: spine enlargement

parallels modification of the number, types and properties of surface glutamate α -amino-3-hydroxy-5-methyl-4-isoxazolepropionic acid (AMPA) receptors during long-term potentiation (LTP), whereas during long-term depression (LTD) the decrease in synaptic strength is associated with spine shrinkage (Kasai *et al.*, 2010).

In this frame, the actin cytoskeleton is important for postsynaptic structure, function and plasticity as it confers spine plasticity and stability (Cingolani and Goda, 2008; Hotulainen and Hoogenraad, 2010; Pelucchi *et al.*, 2020). Actin is highly enriched in spines and filamentous actin (F-actin) is the major structural backbone of spines since it forms organized bundles in spine necks (Star *et al.*, 2002). Only a relatively small fraction of actin in spines is stable (Kasai *et al.*, 2010), while the most abundant dynamic fraction of the actin cytoskeleton provides the driving force behind structural remodelling of spines and contributes to synaptic plasticity (Matus, 2005).

Regulation of actin dynamics is also relevant in Alzheimer's disease pathogenesis, since the signalling pathways influencing actin cytoskeleton remodelling have been shown to be impaired in Alzheimer's Disease (Penzes and Vanleeuwen, 2011; Pelucchi *et al.*, 2020). In particular, among the actin-binding proteins implicated in Alzheimer's disease pathology, cofilin plays a critical role. Indeed, abnormalities of cofilin have been reported in Alzheimer's disease patients (Bamburg and Bernstein, 2016) and β -amyloid oligomers affect cofilin activation (Henriques *et al.*, 2015). Cofilin is a key bi-directional regulator of spine structural plasticity, as it is implicated in both spine enlargement (Bosch *et al.*, 2014) and spine shrinkage (Zhou *et al.*, 2004; Hotulainen *et al.*, 2009; Rust *et al.*, 2010; Pontrello *et al.*, 2012). Cofilin controls F-actin assembly and disassembly in a complex, concentration-dependent manner (Hild *et al.*, 2014; Rust, 2015b). At low concentrations, cofilin promotes F-actin disassembly by accelerating the dissociation of monomeric actin (G-actin) from the filaments' minus ends and by severing F-actin (Blanchoin and Pollard, 1999). Conversely, at high concentrations, cofilin can promote F-actin assembly by nucleating new and by stabilizing pre-existing filaments (Andrianantoandro and Pollard, 2006). Indeed, during LTP cofilin is transported to the spine where it promotes the F-actin assembly that is required for spine expansion (Bosch *et al.*, 2014).

The actin dynamizing activity of cofilin is enhanced by binding partners as the cyclase-associated proteins (CAPs) (Normoyle and Brieher, 2012). CAPs are evolutionary highly conserved multi-domain actin binding proteins capable of regulating actin dynamics at multiple levels (Ono, 2013). Indeed, CAP and cofilin synergize to accelerate the depolymerization of the pointed end of actin filaments (Kotila *et al.*, 2019; Shekhar *et al.*, 2019). CAP deficiency results in defects in vesicle trafficking, endocytosis and in an altered cell morphology and cell growth (Noegel *et al.*, 1999). Two closely related homologs of CAP have been described in mammals. CAP1 is expressed in nearly all cells, whereas CAP2 expression is restricted to a limited number of tissues, including the brain (Bertling *et al.*, 2004; Peche *et al.*, 2007), suggesting that CAP2 may have unique roles, particularly in neuronal cells. CAP2 gene deletion has been described in a rare developmental disorder, named 6p22 syndrome, which is characterized by developmental delays and autism spectrum disorders (Field *et al.*, 2015). In addition, alterations in spine morphology and dendrite architecture have been reported in CAP2 knock-out neurons (Kumar *et al.*, 2016).

Here, we introduce a novel mechanism, altered in both Alzheimer's disease patients and APP/PS1 mice hippocampi, through which the dimerization of CAP2, dependent on Cys³², is relevant for actin dynamics and is necessary to target cofilin to spines upon LTP induction. The mutation of CAP2 Cys³² is sufficient to prevent the

LTP-triggered changes in spine morphology and function. These findings may open new ways in our understanding and targeting synaptic dysfunction and spine dysmorphogenesis in Alzheimer's disease.

Materials and methods

Human brain tissue

The hippocampus and superior frontal gyrus (SFG) samples of Alzheimer's disease patients and of age-matched healthy controls (HC) were obtained from the Netherlands Brain Bank (NBB). Established Braak and Braak criteria were used to categorize Alzheimer's disease tissues (Braak and Braak, 1991). Alzheimer's disease patients fulfilled Braak 4 and 5 stages. Accordingly, in Alzheimer's disease cases, there were tangles and neuritic plaques in hippocampus. HC had no history of psychiatric or neurological disease. Detailed information is reported in Tables 1 and 2.

Triton-insoluble fraction synaptic membrane preparation

Triton insoluble fraction (TIF), a fraction highly enriched in all categories of postsynaptic density proteins (i.e. receptor, signalling, scaffolding and cytoskeletal elements) absent of presynaptic markers (Gardoni *et al.*, 2001), was obtained from human hippocampus and SFG specimens and APP/PS1 and wild-type (WT) hippocampal samples. In order to avoid protein degradation, Alzheimer's disease samples were paired to HC samples and processed at the same time. The procedure was performed at least twice to have two experimental replicates.

Samples of human hippocampal and SFG specimens were homogenized at 4°C in an ice-cold buffer with Roche cOmplete™ Protease Inhibitor Cocktail, Ser/Thr and Tyr phosphatase inhibitors (Sigma-Aldrich), 0.32 M Sucrose, 1 mM Hepes, 1 mM NaF, 0.1 mM PMSF, 1 mM MgCl₂ using a glass-teflon homogenizer. An aliquot of homogenate (Homo) was kept for western blot (WB) analysis. Homo were then centrifuged at 1000 g for 5 min at 4°C, to remove nuclear contamination and white matter. The supernatant was collected and centrifuged at 13 000 g for 15 min at 4°C. The resulting pellet (crude membrane fraction) was resuspended in resuspension buffer [1 mM Hepes with protease inhibitors (Roche cOmplete™)] and then centrifuged at 100 000 g for 1 h at 4°C. Triton-X extraction of the resulting pellet was carried out at 4°C for 15 min in an extraction buffer [1% Triton-X, 75 mM KCl and protease inhibitors (Roche cOmplete™ Protease Inhibitor Cocktail)]. After extraction, the samples were centrifuged at 100 000 g for 1 h at 4°C and the TIFs obtained were resuspended in 20 mM HEPES with protease inhibitors (Roche cOmplete™ Protease Inhibitor Cocktail).

Table 1 Demographic and neuropathological characteristics of Alzheimer's disease and HC cases that were selected for the analysis of hippocampal specimens

Subjects	Gender	Age at death (years)	PMD (hours)	pH CSF	Brain weight (g)	Braak level
1 (AD)	M	82	5.15	6.34	1182	5
2 (AD)	F	84	5.55	6.42	1017	5
3 (AD)	F	88	6.45	6.5	1148	5
4 (AD)	F	91	6.25	6.05	1026	4
5 (AD)	M	90	5.55	6.37	1080	4
6 (AD)	M	91	4.1	6.28	1117	4
7 (AD)	F	86	4.10	6.34	1083	4
8 (AD)	M	81	4.05	6.42	1253	4
9 (AD)	F	86	5.5	6.85	950	4
	Mean ± STD	86.56 ± 3.75	5.19 ± 0.92	6.40 ± 0.21	1095 ± 92.24	
1 (HC)	F	85	6.25	6.6	1080	3
2 (HC)	F	89	6.35	6.73	1139	3
3 (HC)	F	91	4.1	6.58	1052	3
4 (HC)	M	83	5.15	6.6	1372	1
5 (HC)	M	80	4.25	6.59	1429	2
6 (HC)	M	89	6.5	6.23	1185	2
7 (HC)	F	81	6.40	7.16	1164	1
8 (HC)	M	80	7.15	5.8	1376	0
9 (HC)	F	85	4.40	6.71	1165	2
	Mean ± STD	84.78 ± 4.15	5.62 ± 1.15	6.56 ± 0.37	1218 ± 138.23	

AD = Alzheimer's disease; CSF = cerebrospinal fluid; F = female; HC = healthy controls; M = male; PMD = postmortem delay; STD = standard deviation.

Table 2 Demographic and neuropathological characteristics of Alzheimer's disease and HC cases that were selected for the analysis of SFG specimens

Subjects	Gender	Age at death (years)	PMD (hours)	pH CSF	Brain weight (g)	Braak level
1 (AD)	F	91	3.45	6.36	1011	4
2 (AD)	F	91	4.15	6.27	1202	4
3 (AD)	F	86	4.10	6.34	1083	4
4 (AD)	F	86	5.05	6.62	998	4
5 (AD)	M	81	4.05	6.42	1253	4
6 (AD)	F	86	5.5	6.85	950	4
	mean ± STD	86.83 ± 3.76	4.38 ± 0.75	6.48 ± 0.22	1082 ± 120	
1 (HC)	F	84	4.45	6.26	1179	1
2 (HC)	F	81	6.40	7.16	1164	1
3 (HC)	M	80	7.15	5.8	1376	0
4 (HC)	M	84	7.05	5.9	1385	1
5 (HC)	F	85	5.00	6.72	1257	1
6 (HC)	F	85	4.40	6.71	1165	2
	mean ± STD	83.17 ± 2.14	5.74 ± 1.28	6.43 ± 0.53	1254 ± 103	

AD = Alzheimer's disease; CSF = cerebrospinal fluid; F = female; HC = healthy controls; M = male; PMD = postmortem delay; STD = standard deviation.

To obtain the TIF fractions from mouse hippocampi and hippocampal cultures, we used a slightly modified protocol according to the lower amount of tissue. The samples were homogenized at 4°C in a the ice-cold buffer described above using a glass-teflon homogenizer for tissues and a glass-glass homogenizer for the cultures samples. An aliquot of Homo was kept for WB analysis. Homo samples were centrifuged at 13 000 g for 15 min at 4°C. Triton-X extraction of the resulting pellet was carried out at 4°C for 15 min in an extraction buffer [0.5% Triton-X, 75 mM KCl and protease inhibitors (Roche cOmplete™ Protease Inhibitor Cocktail)]. After extraction, the samples were centrifuged at 100 000 g for 1 h at 4°C and the TIFs obtained were resuspended in

20 mM HEPES with protease inhibitors (Roche cOmplete™ Protease Inhibitor Cocktail).

Treatments of neuronal cultures

To induce chemical LTP (cLTP), hippocampal neuronal cultures were first incubated in artificial cerebrospinal fluid (ACSF) for 30 min: 125 mM NaCl, 2.5 mM KCl, 1 mM MgCl₂, 2 mM CaCl₂, 33 mM D-glucose and 25 mM HEPES (pH 7.3; 320 mosM final), followed by stimulation with 50 μM forskolin, 0.1 μM rolipram and 100 μM picrotoxin (Tocris) in ACSF without MgCl₂. After 16 min of stimulation, neurons were replaced in regular ACSF for 15 min and, after treatment, samples

were processed (Marcello *et al.*, 2013). To induce chemical LTD (cLTD), neuronal cultures were incubated in ACSF for 30 min, followed by stimulation with 50 μ M NMDA (Sigma-Aldrich) in ACSF. After 10 min of stimulation, neurons were replaced in regular ACSF for 20 min and then subjected to the biochemical and imaging studies (Marcello *et al.*, 2013). Stimulation of synaptic NMDA receptors (synaptic stimulation) was obtained by treating hippocampal neurons with 50 mM Bicuculline (Tocris), 2.5 mM 4-AP and 5 mM ifenprodil in Neurobasal medium supplemented with B27 (Dinamarca *et al.*, 2016).

Co-immunoprecipitation assays

Aliquots of 20 μ g of TIF obtained from human hippocampus were incubated with an antibody against cofilin overnight at 4°C in a final volume of 150 μ L of RIA buffer [200 mM NaCl, 10 mM ethylene-diaminetetra-acetic acid (EDTA), 10 mM Na₂HPO₄, 0.5% NP-40, 0.1% sodium dodecyl sulfate (SDS)]. SureBeads Protein A/G Magnetic Beads (Bio-Rad) were used to precipitate the immunocomplex. After 3 washes with RIA buffer, the beads were resuspended in sample buffer without β -mercaptoethanol and heated for 3 min before the loading onto SDS-PAGE to detect CAP2 dimer and monomer. Beads were collected by centrifugation and applied onto SDS-PAGE; the precipitated immunocomplex was revealed by anti-cofilin and anti-CAP2 antibody. Heterologous co-immunoprecipitation experiments were carried out from lysates of either COS-7 or HEK293 cells transfected with different combinations of Myc-CAP2, EGFP-CAP2 or EGFP tagged truncated constructs of CAP2. Cells were harvested and proteins extracted as previously described (Marcello *et al.*, 2010). The same immunoprecipitation protocol was used, incubating aliquots of 100 μ g of HEK293/COS-7 lysates with an anti-Myc antibody. Protein A/G Agarose beads (Pierce) were added, and incubation was continued for 2 h at room temperature on the rotator mixer. Beads were collected and washed with RIA buffer for three times. Sample buffer for SDS-PAGE was added and the mixture was heated for 10 min. The precipitated immunocomplex was revealed with either anti-GFP or anti-Myc or anti-actin antibodies.

In situ proximity ligation assay

Proximity ligation assay (PLA) was performed in primary neuronal cultures as previously described (Dinamarca *et al.*, 2016). Primary hippocampal neurons were fixed with 4% paraformaldehyde (PFA)—4% sucrose in PBS for 5 min at 4°C and washed several times with PBS. Neurons were permeabilized with 0.1% Triton X-100 in PBS for 15 min at RT. After incubation with the blocking solution of the PLA kit (Duolink[®] PLA Technology), cells

were incubated overnight with the primary antibodies at 4°C. According to the manufacturer's instructions, after several washing with solution A, secondary probes attached to oligonucleotides were added and the oligonucleotides of the bound probes were ligated and amplified by a fluorescent polymerase that visualizes the PLA signal. To stain MAP2 or the transfected GFP, cells were washed with PBS for 30 min and then the immunocytochemistry protocol was used. Cells were mounted on slides in Fluoromount[™] Aqueous Mounting Medium (Sigma-Aldrich).

Cell culture electrophysiology

Whole cell voltage-clamp recordings were performed on rat hippocampal neurons transfected at day *in vitro* (DIV) 10 and maintained in culture for 15–16 DIV. Recording pipettes were fabricated from borosilicate glass capillary with a tip resistance of 3–5 M Ω and filled with an intracellular solution of the following composition (in mM): 130 potassium gluconate, 10 KCl, 1 EGTA, 10 Hepes, 2 MgCl₂, 4 MgATP and 0.3 Tris-GTP. During recordings of miniature excitatory postsynaptic currents (mEPSCs), cells were bathed in a standard external solution containing (in mM): 125 NaCl, 5 KCl, 1.2 MgSO₄, 1.2 KH₂PO₄, 2 CaCl₂, 6 glucose and 25 HEPES-NaOH, pH 7.4, with also tetrodotoxin (TTX-1 μ M), bicuculline (20 μ M) and strychnine (1 μ M). For chemical LTP experiments, recordings of mEPSCs were performed applying glycine (100 μ M) for 3 min at room temperature in Mg²⁺-free KRH, also containing TTX, bicuculline and strychnine. Recordings were performed at room temperature in voltage clamp mode using a Multiclamp 700B amplifier (Molecular Devices) and pClamp-10 software (Axon Instruments). Series resistance ranged from 10 M Ω to 20 M Ω and was monitored for consistency during recordings. Cells in culture with leak currents >200 pA were excluded from the analysis. Signals were amplified, sampled at 10 kHz, filtered to 2 or 3 kHz and analyzed using pClamp 10 data acquisition and analysis program.

Ethical approvals

All procedures performed in studies involving human participants were in accordance with the ethical standards of the institutional research committee (Brescia Ethics Committee, protocol #NP2806) and with the 1964 Helsinki declaration and its later amendments or comparable ethical standards.

All procedures performed in studies involving animals were in accordance with the ethical standards of the Institutional Animal Care and Use Committee of University of Milan (Italian Ministry of Health permit #326/2015, #5247B.N.YCK/2018, #295/2012-A, #497/2015-PR) and of the internal animal welfare authorities of the University of Marburg (references: AK-6-2014-

Rust), at which the studies were conducted. Animals were maintained on a 12-h light/dark cycle in a temperature-controlled room (22°C) in cages with free access to food and water. Housing in the animal facility is performed in conformity with local and European Community regulations under the control of veterinarians with the assistance of trained personnel.

Experimental design and quantification of data

To minimize the possibility of bias in experimental results, randomization and blinding were used in the experimental design, imaging acquisitions and analyses. Acquisition and quantification of western blotting was performed by means of computer-assisted imaging (ChemiDoc system and Image lab 4.0 software; Bio-Rad). Data obtained by coimmunoprecipitation assays were normalized on the amount of immunoprecipitated protein. As far as concern imaging analysis, cells were randomly chosen from at least two cultures. Morphological analysis of dendritic spines was performed on the total length of the dendrites using ImageJ software to measure spine length, head and neck width (Malinverno et al., 2010). Sholl analysis was performed using Fiji free software as described in Mauceri et al. (2011).

Cofilin spine localization analysis was carried out assuming that the spine volume and the amount of fusion protein were proportional to the integrated intensity of the RFP signal (Bosch et al., 2014). Z-stack images were processed and analysed using Nikon Elements software and ImageJ. To analyse the distribution of PSD-95 and Bassoon within the spine, a line was drawn across the spine head semi-perpendicular to the dendrite, and the proteins intensity profiles were evaluated (Smith et al., 2014). The analysis of PLA experiments was performed with ImageJ software and the number of clusters was normalized on the total dendritic length. Total internal reflection fluorescence image analysis was done using Fiji. For spontaneous depolymerization, kymographs of single filaments (30–50 filaments per condition) were generated and depolymerization rates were calculated from the slope of the graphs. To assess cofilin cutting rates, at least 30 filaments in the frame were selected.

Statistical analysis

Linear mixed-effects (LMMs) models were used in most of the imaging experiments (Tables 3 and 4) as outcome variables were mostly continuous. To account for the hierarchical structure of dendritic spine morphology designs, we specified one mixed-effects model (Pinheiro and Bates, 2006) for each experiment under investigation and outcome variable of interest within the experiment (Paternoster et al., 2018). Generalized linear mixed-effects models with a logit link function and binomial family

were fitted for the Type outcome variable in the experiments assessing spine morphology; in these analyses, the outcome variable was restricted to assume categories Mushroom (reference category) and Stubby only. For each mixed-effects model, one or two random intercepts were specified depending on the available levels of the hierarchy. The culture random intercept was present in any model, whereas the neuron level of the hierarchy was present when the experimental unit of analysis was spine and it was not estimable when neuron itself was the experimental unit. Correlations between random effects were allowed to be present and fitted within the model to better capture the hierarchical structure of the experiment. We reported information on which dependent and independent variables were used within each mixed-effects model in Table 3 (columns on the left). For model fitting, restricted maximum likelihood (REML) estimates were used, as they provided better estimates of variance components. To test model assumptions, we plotted residuals versus fitted values for each model; when outliers were detected, they were checked at the experimental level. When model convergence issues persisted after changing the estimation method, we fitted an equivalent model showing a fixed-effects term instead of the corresponding mixed-effect one. If two hierarchical levels were available in the experiment, the fitted model was still a mixed-effects model splitting the hierarchical levels into one random- and one fixed-effect term; when neuron was the experimental unit, a fixed-effects model was estimated using ordinary least squares method. Hypothesis testing on the significance of single parameters was performed within the linear mixed-effects or generalized linear mixed-effects models with a Student *t* distribution or a Gaussian distribution, respectively. The F statistics from the ANOVA analysis provided information on the overall significance of the independent variables entered into each model. When necessary, contrasts of interest were extracted from the linear mixed-effects to calculate estimated mean differences and Standard errors (SEs) between any pair of categories of the effect of interest. The corresponding *P*-values were adjusted for multiple comparisons according to the False Discovery Rate (FDR) or Benjamini–Hochberg method (Table 4) (Benjamini and Hochberg, 1995). Finally, the chi-squared test of independence was used to assess the presence of an association between spine type and genetic modification.

For all the other experiments, as data followed a normal distribution, either Student *t*-test or one-way ANOVA, followed by a *post hoc* adjustment, were carried out.

Throughout the manuscript, when continuous variables were considered, values were reported as mean \pm SE, and when qualitative variables were analysed, absolute frequencies (raw numbers) or percentages were indicated. The type of parametric test used for each experiment and the corresponding *P*-values, as well the type of

Table 3 Estimates of the mean and standard error from mixed-effects models fitted to the available datasets of the corresponding figures

Figure	Y	Random effects at different hierarchical levels		Variable	Estimate	Standard error	P value							
		Culture	Neuron											
3 B, C	Spine length	n = 2 STD = 0.0853	$\eta_{SCR} = 8$, $\eta_{CAP2-shRNA} = 7$ STD = 0.0504	Genetic modification CAP2-shRNA versus SCR ANOVA, $P < 0.0001$	0.1657	0.0181	<0.0001							
								Spine width	n = 2 STD = 0.0163	$\eta_{SCR} = 8$, $\eta_{CAP2-shRNA} = 7$ STD = 0.031	Genetic modification CAP2-shRNA versus SCR ANOVA, $P < 0.0001$	0.0312	0.0087	0.00035
3 E, F	Dendritic length	n = 2 STD = 0.3081	N/E ^b	Genetic modification CAP2-shRNA versus SCR ANOVA, $P = 0.4995$	-299.67	136.12	0.4995							
								Intersection	n = 2 STD = 0.8726	Culture, ANOVA, $P = 0.7505$ Genetic modification CAP2-shRNA, ANOVA, $P = 0.4457$ Length, ANOVA, $P < 0.0001$ Culture, ANOVA, $P = 0.7804$	44.85 -0.5065 0.0627 0.0892	137.53 0.6634 0.0075 0.3199	0.75 0.4457 <0.0001 0.7803	
5 F	PLA clusters/ μ m	n = 2 STD = 0.3081	N/E ^b	Interaction between genetic modification and length, ANOVA, $P = 0.0394$ Genetic modification EGFP-CAP2/Myc-(C32G)CAP2 versus EGFP-CAP2/Myc-CAP2 ANOVA, $P < 0.0001$	-0.0219 -0.7997	0.0106 0.1486	0.0394 <0.0001							
6 G	PLA clusters/ μ m	n = 3 STD = 0.3081	N/E ^b	Genetic modification Myc-(C32G)CAP2 versus Myc-CAP2 ANOVA, $P = 0.0146$	-0.0176	0.0064	0.0126							
								PLA clusters/ μ m	n = 2 STD = 0.075	Culture 2, ANOVA, $P = 0.2579$ Culture 3, ANOVA, $P = 0.2579$ MycCAP2 and cLTP Myc-(C32G) CAP2 and CTRL Myc-(C32G) CAP2 and cLTP ANOVA, $P < 0.0001$	-0.0070 0.0074 0.5791 -0.5914 -0.6388	0.0075 0.0078 0.1640 0.177 0.177	0.3670 0.3556 0.00086 0.0016 0.00070	
7 H	PLA clusters/ μ m	n = 2 STD = 0.0031	N/E ^b	Myc-CAP2 and cLTP Myc-(C32G) CAP2 and CTRL Myc-(C32G) CAP2 and cLTP ANOVA, $P < 0.0001$	0.0668 -0.0178 -0.0001	0.0096 0.0104 0.0096	<0.0001 0.0960 0.9901							
8 B	IntDen Cofilin/IntDen RFP	n = 2 STD = 0.03599	$\eta_{SCR-CTRL} = 13$ $\eta_{SCR-LTP} = 13$ $\eta_{CAP2-shRNA-LTP} = 11$ $\eta_{shr-wt-CAP2-LTP} = 11$ $\eta_{shr-C32G-CAP2-LTP} = 10$ STD = 0.1167	Genetic modification and treatment, CAP2-shRNA and cLTP Genetic modification and treatment, SCR and cLTP Genetic modification and treatment, shRNA + shr-C32G-CAP2 and cLTP Genetic modification and treatment, shRNA + shr-wt-CAP2 and cLTP ANOVA, $P < 0.0001$	0.0051 0.0992 0.0244 0.1386	0.0243 0.0218 0.0240 0.0239	0.833 <0.0001 0.309 <0.0001							

(continued)

Table 3 Continued

Figure	Y	Random effects at different hierarchical levels		Variable	Estimate	Standard error	P value						
		Culture	Neuron										
8 D, E	Spine length	n = 2 STD = 0.1197	$\eta_{SCR-CTRL} = \text{II}$	Genetic modification and treatment, CAP2-shRNA, and cLTP	0.3468	0.0173	<0.0001						
			$\eta_{SCR-LTP} = \text{II}$					Genetic modification and treatment, SCR and cLTP					
			$\eta_{CAP2-shRNA-LTP} = \text{II}$					Genetic modification and treatment, shRNA + shir-C32G-CAP2 and cLTP					
			$\eta_{shir-wt-CAP2-LTP} = \text{II}$					Genetic modification and treatment, shRNA + shir-wt-CAP2 and cLTP					
			$\eta_{shir-C32G-CAP2-LTP} = \text{II}$					ANOVA P < 0.0001					
			STD = 0.0620										
			$\eta_{SCR-CTRL} = \text{II}$					Genetic modification and treatment, CAP2-shRNA, and cLTP	0.0116	0.0094	0.2119		
			$\eta_{SCR-LTP} = \text{II}$									Genetic modification and treatment, SCR and cLTP	
			$\eta_{CAP2-shRNA-LTP} = \text{II}$									Genetic modification and treatment, shRNA + shir-C32G-CAP2 and cLTP	
			$\eta_{shir-wt-CAP2-LTP} = \text{II}$									Genetic modification and treatment, shRNA + shir-wt-CAP2 and cLTP	
$\eta_{shir-C32G-CAP2-LTP} = \text{II}$	ANOVA P < 0.0001												
STD = 0.0474													
$\eta_{SCR-CTRL} = \text{II}$	Genetic modification and treatment, CAP2-shRNA, and cLTP	-0.7528	0.1077	<0.0001									
$\eta_{SCR-LTP} = \text{II}$					Genetic modification and treatment, SCR and cLTP								
$\eta_{CAP2-shRNA-LTP} = \text{II}$					Genetic modification and treatment, shRNA + shir-C32G-CAP2 and cLTP								
$\eta_{shir-wt-CAP2-LTP} = \text{II}$					Genetic modification and treatment, shRNA + shir-wt-CAP2 and cLTP								
$\eta_{shir-C32G-CAP2-LTP} = \text{II}$					ANOVA P < 0.0001								
STD = 0.283													
Spine width					n = 2 STD = 0.0254	$\eta_{SCR-CTRL} = \text{II}$	Genetic modification and treatment, CAP2-shRNA, and cLTP	0.0116	0.0094	0.2119			
						$\eta_{SCR-LTP} = \text{II}$					Genetic modification and treatment, SCR and cLTP		
						$\eta_{CAP2-shRNA-LTP} = \text{II}$					Genetic modification and treatment, shRNA + shir-C32G-CAP2 and cLTP		
						$\eta_{shir-wt-CAP2-LTP} = \text{II}$					Genetic modification and treatment, shRNA + shir-wt-CAP2 and cLTP		
	$\eta_{shir-C32G-CAP2-LTP} = \text{II}$	ANOVA P < 0.0001											
	STD = 0.0474												
	Spine type	n = 2 ^a	$\eta_{SCR-CTRL} = \text{II}$	Genetic modification and treatment, CAP2-shRNA, and cLTP		-0.7528					0.1077	<0.0001	
			$\eta_{SCR-LTP} = \text{II}$										Genetic modification and treatment, SCR and cLTP
			$\eta_{CAP2-shRNA-LTP} = \text{II}$										Genetic modification and treatment, shRNA + shir-C32G-CAP2 and cLTP
			$\eta_{shir-wt-CAP2-LTP} = \text{II}$										Genetic modification and treatment, shRNA + shir-wt-CAP2 and cLTP
$\eta_{shir-C32G-CAP2-LTP} = \text{II}$			ANOVA P < 0.0001										
STD = 0.283													
Culture			n = 2 ^a		$\eta_{SCR-CTRL} = \text{II}$		Genetic modification and treatment, CAP2-shRNA, and cLTP	-0.7528	0.1077	<0.0001			
					$\eta_{SCR-LTP} = \text{II}$								Genetic modification and treatment, SCR and cLTP
					$\eta_{CAP2-shRNA-LTP} = \text{II}$								Genetic modification and treatment, shRNA + shir-C32G-CAP2 and cLTP
					$\eta_{shir-wt-CAP2-LTP} = \text{II}$								Genetic modification and treatment, shRNA + shir-wt-CAP2 and cLTP
	$\eta_{shir-C32G-CAP2-LTP} = \text{II}$	ANOVA P < 0.0001											
	STD = 0.283												
	Culture	n = 2 ^a		$\eta_{SCR-CTRL} = \text{II}$	Genetic modification and treatment, CAP2-shRNA, and cLTP	-0.7528					0.1077	<0.0001	
				$\eta_{SCR-LTP} = \text{II}$									Genetic modification and treatment, SCR and cLTP
				$\eta_{CAP2-shRNA-LTP} = \text{II}$									Genetic modification and treatment, shRNA + shir-C32G-CAP2 and cLTP
				$\eta_{shir-wt-CAP2-LTP} = \text{II}$									Genetic modification and treatment, shRNA + shir-wt-CAP2 and cLTP
$\eta_{shir-C32G-CAP2-LTP} = \text{II}$			ANOVA P < 0.0001										
STD = 0.283													
Culture			n = 2 ^a	$\eta_{SCR-CTRL} = \text{II}$			Genetic modification and treatment, CAP2-shRNA, and cLTP	-0.7528	0.1077	<0.0001			
				$\eta_{SCR-LTP} = \text{II}$									Genetic modification and treatment, SCR and cLTP
				$\eta_{CAP2-shRNA-LTP} = \text{II}$									Genetic modification and treatment, shRNA + shir-C32G-CAP2 and cLTP
				$\eta_{shir-wt-CAP2-LTP} = \text{II}$									Genetic modification and treatment, shRNA + shir-wt-CAP2 and cLTP
	$\eta_{shir-C32G-CAP2-LTP} = \text{II}$	ANOVA P < 0.0001											
	STD = 0.283												

The hierarchical structure of the experiments was introduced in the left part of the table, including the standard deviation (STD) of the random-effects terms when available.

^aDue to convergence issues, fixed-effects terms were introduced instead of the corresponding mixed-effects ones for some hierarchical levels.

^bN/E = not estimable due to the presence of one hierarchical level only (i.e. neuron is the experimental unit).

Table 4 Pairwise contrasts of interest derived from mixed-effects models introduced in **Figs 7 and 8**

Figure	Y	Contrast	Estimate	Standard error	P value
7 F	PLA clusters/ μm	EGFP-CAP2/Myc-(C32G)CAP2-CTRL versus EGFP-CAP2/Myc-CAP2-CTRL	-0.5914	0.1777	<0.0001
		EGFP-CAP2/Myc-(C32G)CAP2-cLTP versus EGFP-CAP2/Myc-CAP2-CTRL	-0.6388	0.1777	0.00129
		EGFP-CAP2/Myc-CAP2-cLTP versus EGFP-CAP2/Myc-CAP2-CTRL	0.5791	0.1640	0.00129
		EGFP-CAP2/Myc-(C32G)CAP2-cLTP versus EGFP-CAP2/Myc-(C32G)CAP2-CTRL	-0.0475	0.1894	0.8030
		EGFP-CAP2/Myc-CAP2-cLTP versus EGFP-CAP2/Myc-(C32G)CAP2-CTRL	1.1705	0.1777	<0.0001
7 H	PLA clusters/ μm	EGFP-CAP2/Myc-CAP2(C32G)-cLTP versus EGFP-CAP2/Myc-CAP2-cLTP	-1.2180	0.1777	<0.0001
		Myc-(C32G)CAP2/Cofilin-CTRL versus Myc-CAP2/Cofilin-CTRL	-0.0178	0.0104	0.115
		Myc-(C32G)CAP2/Cofilin-cLTP versus Myc-CAP2/Cofilin-CTRL	-0.0001	0.0096	0.9901
		Myc-CAP2/Cofilin-cLTP versus Myc-CAP2/Cofilin-CTRL	0.0668	0.0096	<0.0001
		Myc-(C32G)CAP2/Cofilin-cLTP versus Myc-(C32G)CAP2/Cofilin-CTRL	0.0177	0.0102	0.115
8 B	IntDen Cofilin/IntDen RFP	Myc-(C32G)CAP2/Cofilin-cLTP versus Myc-(C32G)CAP2/Cofilin-CTRL	0.0846	0.0102	<0.0001
		Myc-(C32G)CAP2/Cofilin-cLTP versus Myc-CAP2/Cofilin-cLTP	-0.0669	0.0094	<0.0001
		CAP2-shRNA-cLTP versus SCR-CTRL	-0.0051	0.0243	0.834
		SCR-cLTP versus SCR-CTRL	0.0992	0.0218651	<0.0001
		shRNA + shr-C32G-CAP2-cLTP versus SCR-CTRL	0.0245	0.0240298	0.386
		shRNA + shr-wt-CAP2-cLTP versus SCR-CTRL	0.1386	0.0239044	<0.0001
		CAP2-shRNA-cLTP versus SCR-cLTP	-0.09412	0.0236968	0.00016
		CAP2-shRNA-cLTP versus shRNA + shr-C32G-CAP2-cLTP	-0.01937	0.0250532	0.489
		CAP2-shRNA-cLTP versus shRNA + shr-wt-CAP2-cLTP	-0.1335	0.0238909	<0.0001
		shRNA + shr-C32G-CAP2-cLTP versus SCR-cLTP	-0.07475	0.0233884	0.00246
8 D	Spine length	shRNA + shr-wt-CAP2-cLTP versus SCR-cLTP	0.0394	0.0231644	0.128
		shRNA + shr-C32G-CAP2-cLTP versus shRNA + shr-wt-CAP2-cLTP	-0.1142	0.0240324	<0.0001
		CAP2-shRNA-cLTP versus SCR-CTRL	0.3468	0.0173	<0.0001
		SCR-cLTP versus SCR-CTRL	0.2984	0.0177	<0.0001
		shRNA + shr-C32G-CAP2-cLTP versus SCR-CTRL	0.3676	0.0165	<0.0001
		shRNA + shr-wt-CAP2-cLTP versus SCR-CTRL	0.1881	0.0184	<0.0001
		CAP2-shRNA-cLTP versus SCR-cLTP	0.0484	0.0180	0.00795
		shRNA + shr-C32G-CAP2-cLTP versus CAP2-shRNA-cLTP	0.0207	0.0171	0.2255
		shRNA + shr-wt-CAP2-cLTP versus CAP2-shRNA-cLTP	-0.1588	0.0187	<0.0001
		shRNA + shr-C32G-CAP2-cLTP versus SCR-cLTP	0.0691	0.0171	<0.0001
	Spine width	shRNA + shr-wt-CAP2-cLTP versus SCR-cLTP	-0.1104	0.0187	<0.0001
		shRNA + shr-C32G-CAP2-cLTP versus shRNA + shr-wt-CAP2-cLTP	0.1795	0.0184	<0.0001
		CAP2-shRNA-cLTP versus SCR-CTRL	0.0116	0.0094	0.2185
		SCR-cLTP versus SCR-CTRL	0.2100	0.0096	<0.0001
		shRNA + shr-C32G-CAP2-cLTP versus SCR-CTRL	-0.0473	0.0090	<0.0001
		shRNA + shr-wt-CAP2-cLTP versus SCR-CTRL	0.2821	0.0100	<0.0001
		CAP2-shRNA-cLTP versus SCR-cLTP	-0.1984	0.0098	<0.0001
		shRNA + shr-C32G-CAP2-cLTP versus CAP2-shRNA-cLTP	-0.0589	0.0093	<0.0001
		shRNA + shr-wt-CAP2-cLTP versus CAP2-shRNA-cLTP	0.2705	0.0102	<0.0001
		shRNA + shr-C32G-CAP2-cLTP versus SCR-cLTP	-0.2573	0.0093	<0.0001
shRNA + shr-wt-CAP2-cLTP versus SCR-cLTP	0.0721	0.0102	<0.0001		
shRNA + shr-C32G-CAP2-cLTP versus shRNA + shr-wt-CAP2-cLTP	-0.3294	0.0100	<0.0001		

P values were derived after adjustment for multiple comparisons according to the false discovery rate (FDR) approach.

adjustment for multiple comparisons (if any), were provided in figure legends. All statistical tests were two-sided and significance was assumed if $P < 0.05$. Calculations were carried out using the open-source statistical computing environment R (R Core Team, 2019) with its libraries lme4 (Bates *et al.*, 2015), lmerTest (Kuznetsova *et al.*, 2017) and emmeans (Lenth, 2020), for the imaging experiments and with Prism 6 (GraphPad, La Jolla, CA, USA) for all the other quantitative evaluations.

Data availability

Data are available on direct request to the corresponding author.

Results

Synaptic localization of CAP2 and cofilin is impaired in Alzheimer's disease hippocampi

The actin-binding protein CAP2, that is expressed in several brain areas including the hippocampus (Supplementary Fig. 1A), has been described as a cofilin binding partner (Kumar *et al.*, 2016). An impaired activation of cofilin has been reported in the hippocampus of Alzheimer's disease patients (Minamide *et al.*, 2000; Barone *et al.*, 2014). Cofilin postsynaptic localization, that plays a crucial role in synaptic plasticity phenomena

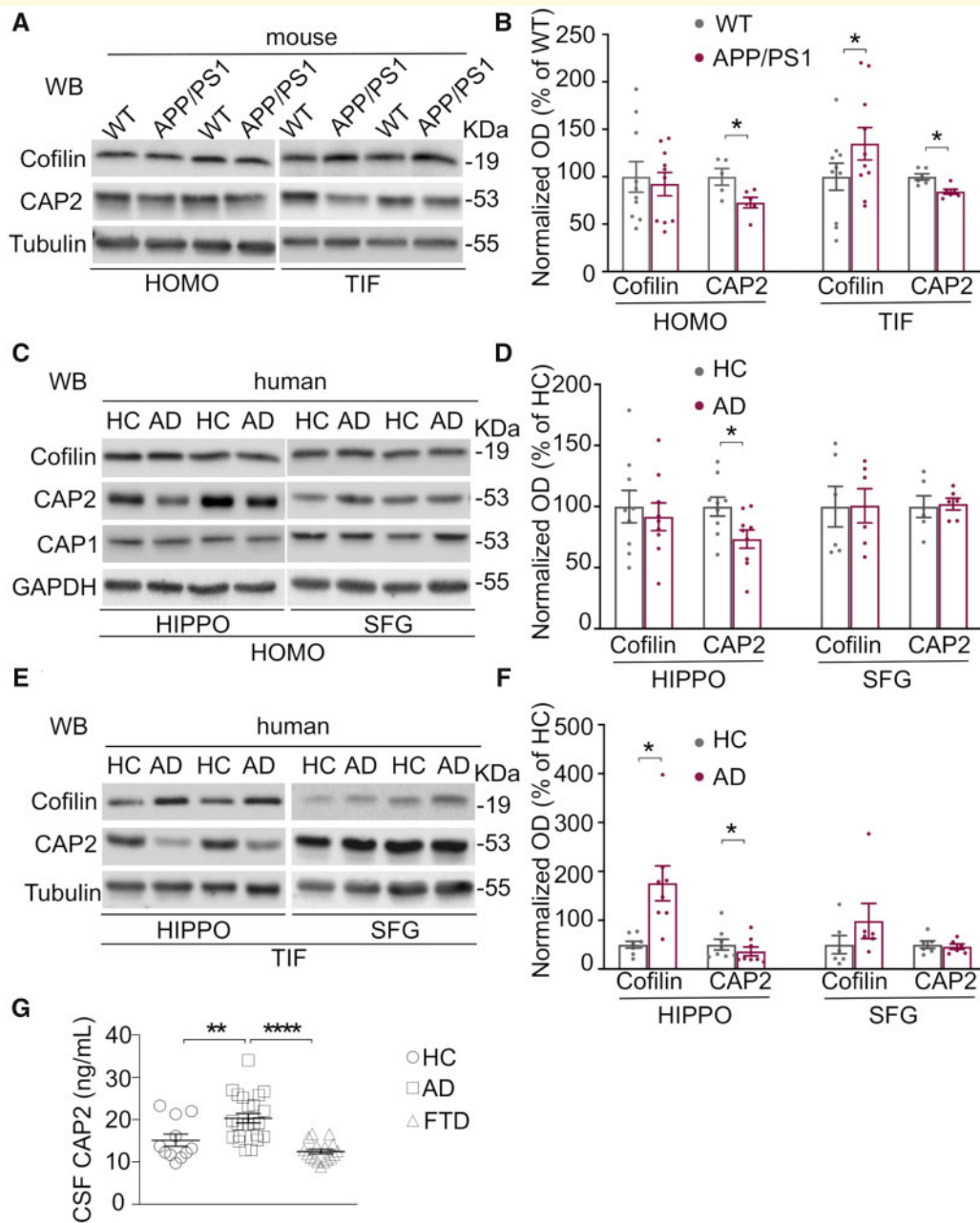


Figure 1 The synaptic localization of cofilin and CAP2 is specifically altered in the hippocampus of Alzheimer's disease patients and APP/PS1 mice. **(A)** Representative WB showing the expression of cofilin, CAP2 and Tubulin in homogenate (HOMO) and TIF hippocampal samples of APP/PS1 mice at 6 months of age compared to wild type (WT) animals. Non-cropped blots are shown in [Supplementary Fig. 1C](#). **(B)** Quantification of optical density (OD) and normalization on loading control OD (Tubulin) shows that CAP2 but not cofilin total levels are reduced in APP/PS1 mice (HOMO, CAP2, APP/PS1 versus WT, unpaired *t*-test: $*P = 0.023$, n WT = 5 mice, n APP/PS1 = 6 mice; cofilin, APP/PS1 versus WT, unpaired *t*-test: $P > 0.05$, n WT = 10 mice, n APP/PS1 = 10 mice). In the TIF fraction, the quantitative analysis reveals that cofilin levels increase in transgenic mice, while CAP2 levels decrease (TIF, cofilin, APP/PS1 versus WT, paired *t*-test: $*P = 0.015$, n WT = 10 mice, n APP/PS1 = 10 mice; CAP2, APP/PS1 versus WT, paired *t*-test: $*P = 0.026$, n WT = 6 mice, n APP/PS1 = 6 mice). **(C)** Representative WB showing the expression of cofilin, CAP2, CAP1 and GAPDH in homogenate samples (HOMO) of Alzheimer's Disease (AD) and HC hippocampi (HIPPO) and SFG. Non-cropped blots are shown in [Supplementary Fig. 1D](#). **(D)** Quantification of optical density (OD) and normalization on loading control OD (GAPDH) shows that CAP2 but not cofilin total levels are reduced in AD patients (CAP2, AD versus HC, unpaired *t*-test: $*P = 0.027$, n HC = 9, n AD = 9). In SFG HOMO samples cofilin and CAP2 levels were not affected in AD patients compared to HC (AD versus HC, unpaired *t*-test: $*P > 0.05$, n HC = 6, n AD = 6). No changes in CAP1 levels in the HOMO of both HIPPO and SFG were observed (CAP1, HIPPO, HC = $100 \pm 8.72\%$, AD = $89.83 \pm 9.65\%$ AD versus HC, unpaired *t*-test: $P > 0.05$, n HC = 8, n AD = 9; SFG, HC = $100 \pm 5.35\%$, AD = $110.8 \pm 12.3\%$, AD versus HC, unpaired *t*-test: $P > 0.05$, n HC = 6, n AD = 6). **(E)** Representative WB showing cofilin, CAP2 and Tubulin levels in postsynaptic TIF samples of the HIPPO and SFG of AD and HC. Non-cropped blots are shown in [Supplementary Fig. 1E](#). **(F)** The quantitative analysis reveals that cofilin levels increase in the TIF of AD patients while CAP2 levels decrease (cofilin, AD versus HC, paired *t*-test: $*P = 0.0109$,

(continued)

(Bosch *et al.*, 2014; Mikhaylova *et al.*, 2018), is not altered in the frontal cortex of Alzheimer's disease patients and in the brain of animal models (Rush *et al.*, 2018). Considering that the hippocampus is one of the first brain areas affected in Alzheimer's disease patients (Frisoni *et al.*, 2010), we first assessed total and synaptic levels of cofilin and CAP2 in the hippocampus of APP/PS1 mice at 6 months of age, when they begin to develop amyloid deposits (Jankowsky *et al.*, 2004). We purified the triton-insoluble fraction (TIF), which is highly enriched in postsynaptic proteins (Gardoni *et al.*, 2001). WB analysis performed on the total homogenate and on the TIF samples shows a significant increase in cofilin synaptic levels in APP/PS1 mice hippocampi compared to WT mice, while no changes in the total protein levels were detected (Fig. 1A and B). Interestingly, the CAP2 protein levels in the total homogenate and, consistently, in the postsynaptic fraction of APP/PS1 mice were significantly reduced compared to WT mice (Fig. 1A and B).

These data suggest an altered synaptic availability of cofilin and of its binding partner CAP2 in the hippocampal synapses of APP/PS1 mice at the early stages of the pathology.

To strengthen these results, and verify the relevance in human pathology, we took advantage of autaptic specimens obtained from sporadic Alzheimer's Disease patients, fulfilling criteria for Braak 4 and 5 stage, and age-matched control subjects (HC) (Tables 1 and 2). In particular, we examined hippocampus and SFG, two areas differentially affected by the pathology.

The analysis of the total homogenate revealed no changes in cofilin total protein levels and a significant down-regulation of CAP2 in Alzheimer's disease patients hippocampi (Fig. 1C and D), as previously reported in microarray studies (Blalock *et al.*, 2004). This Alzheimer's disease-associated alteration of CAP2 is specific since no modifications in the total levels of the homolog CAP1 have been detected in Alzheimer's disease patients' hippocampi and SFG when compared to HC (Fig. 1C and D). After the validation of the postsynaptic fraction purification protocol from human specimens (Supplementary Fig. 1B), we performed WB analysis of the TIF samples. A significant increase in cofilin synaptic levels and a concomitant decrease in CAP2 synaptic localization have been detected (Fig. 1E and F), as observed in APP/PS1 hippocampi (Fig. 1A and B). Interestingly, these alterations are specific for the hippocampus because no modifications of CAP2 and cofilin total levels and

synaptic localization were found in SFG (Fig. 1 C–F), consistent with previous data showing no changes of cofilin levels in the postsynaptic densities (PSD) fraction of the frontal cortex of Alzheimer's disease patients (Rush *et al.*, 2018).

Furthermore, we challenged cerebrospinal fluid (CSF) for the presence of CAP2. A preliminary screening experiment of CAP2 levels in the CSF has been performed on 23 Alzheimer's disease patients, 11 HC, 17 frontotemporal dementia patients as non-Alzheimer's disease neurodegenerative controls. CAP2 levels in Alzheimer's disease patients (20.34 ± 1.12 ng/ml) were significantly higher than in HC (15.13 ± 1.45 ng/ml) and in frontotemporal dementia patients (12.45 ± 0.56 ng/ml) (Fig. 1G), suggesting that the changes in CAP2 are specifically associated to Alzheimer's disease.

CAP2 is a synaptic protein relevant for synaptic function and neuronal structure

Since the Alzheimer's disease-related alterations of CAP2 and cofilin have been detected in the postsynaptic compartment, we decided to further investigate CAP2 role in dendritic spines. We employed stimulated emission depletion nanoscopy to analyse primary hippocampal neurons stained for endogenous CAP2, pre- and postsynaptic markers and F-actin, labelled by phalloidin. Endogenous CAP2 has a distribution pattern similar to phalloidin, is localized throughout the dendrites and is detectable in dendritic spines, as previously reported (Kumar *et al.*, 2016) (Supplementary Fig. 2A). A linescan through the spine length shows that peaks of fluorescence for CAP2 and the presynaptic marker Bassoon do not overlap (Fig. 2A), while CAP2 fluorescence profile shows a partial overlap with the postsynaptic protein PSD-95 profile (Fig. 2B) (Smith *et al.*, 2014).

To further confirm the localization of CAP2 in the postsynaptic compartment, we performed biochemical fractionation of rat hippocampi to isolate the PSD. WB analysis demonstrated that CAP2 is present in the synaptic fractions but not enriched in highly detergent-insoluble fractions PSD2, which corresponds to the 'core' of the PSD (Supplementary Fig. 2B).

To gain insights into the specific role of CAP2 in hippocampal neuronal cells and considering the reduction of CAP2 protein levels in the hippocampi of Alzheimer's

Figure 1 Continued

n HC = 8, n AD = 8; CAP2, AD versus HC, paired *t*-test: $*P = 0.0172$, n HC = 8, n AD = 8). No significant modifications of cofilin and CAP2 synaptic localization were detected in the SFG (AD versus HC, paired *t*-test: $*P > 0.05$; n HC = 6, n AD = 6). (G) CSF concentration of CAP2 in healthy controls (HC), Alzheimer's Disease patients (AD) and frontotemporal dementia patients (FTD). CAP2 levels are higher in AD patients, but not in FTD patients, compared to HC (HC: CAP2 = 15.13 ± 1.5 ng/ml, n = 11; AD: CAP2 = 20.34 ± 1.12 ng/ml, n = 23; FTD: CAP2 = 12.45 ± 0.56 ng/ml, n = 17; one-way ANOVA, Bonferroni multiple comparison test: $**P = 0.0075$; $***P < 0.0001$).

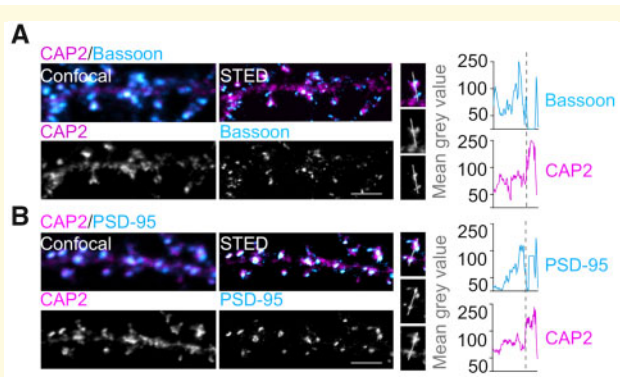


Figure 2 CAP2 is a postsynaptic protein. Confocal and stimulated emission depletion images of hippocampal neurons fixed and stained for CAP2 (magenta) and synaptic markers, either Bassoon (A) or PSD-95 (B) (cyan). Linescan through spine head was used to evaluate the mean grey value of the stained proteins. Scale bar = 2 μ m.

disease patients and APP/PS1 mice (Fig. 1A–D), we took advantage of small hairpin RNA (shRNA) to down-regulate CAP2 expression. We first identified a shRNA that reduced by about 80% the levels of co-transfected Myc-CAP2 in heterologous cells (CAP2-shRNA, Supplementary Fig. 2C). The same shRNA reduced by about 80% endogenous CAP2 mRNA levels when packaged into recombinant adeno-associated virus (rAAV) particles and used to infect primary hippocampal neurons (Supplementary Fig. 2D).

Since CAP2 is a postsynaptic actin binding protein, we investigated whether its down-regulation affects spine morphology and synaptic transmission in hippocampal neurons.

The analysis of the spine shape of hippocampal neurons transfected with CAP2-shRNA and GFP revealed a significant increase in spine length and head width, while no changes in density of spines were detected (Fig. 3A and B, SCR: 2.61 ± 0.30 spines/10 μ m; CAP2-shRNA: 2.65 ± 0.36 spines/10 μ m). The examination of the different spines categories showed that the different spines populations were associated with CAP2-down-regulation (Fig. 3C), highlighting altered neuronal spine morphology in CAP2-shRNA transfected neurons. Notably, in primary hippocampal neurons transfected with CAP2-shRNA and GFP, to visualize dendrite architecture, the Sholl analysis revealed a reduction in the complexity of the dendritic tree (Fig. 3D and F). This effect was accompanied by a significant reduction in total dendritic length (Fig. 3E). Interestingly, the down-regulation of CAP2 levels also reduces the mRNA levels of BDNF, a neurotrophin that controls dendrite morphology (Horch and Katz, 2002) (Supplementary Fig. 2D). These data suggest that the down-regulation of CAP2 affects neuronal architecture and spine morphology. Therefore, we asked whether the decreased CAP2 expression could influence synaptic

function. Firstly, we observed that the knockdown of CAP2 impairs the expected increase in the transcription of immediate early genes (cFos and Arc) after the induction of both chemical LTP (cLTP) and synaptic stimulation (Fig. 3G). This suggests the relevance of CAP2 in synaptic plasticity phenomena and is consistent with an alteration of neuronal architecture leading to impaired integration of signal-regulated transcription. Secondly, we recorded the miniature excitatory postsynaptic currents (mEPSCs) in neurons that revealed impairments in the post-synaptic AMPA receptors sensitivity as suggested by the lower mEPSCs amplitude in CAP2-shRNA neurons respect to control conditions (Fig. 3H and I). To assess whether this effect could be specifically ascribed to CAP2, we generated and validated a shRNA-resistant (shr) ‘rescue’ form of Myc-CAP2 (shr-wt-CAP2) that was insensitive to the CAP2-shRNA (Supplementary Fig. 2E). As shown in Fig. 3I, the mEPSCs amplitude was restored to control levels by the shr-wt-CAP2, demonstrating the specificity of the effect on synaptic transmission. These results indicate that the down-regulation of CAP2 leads to a less responsive/functional postsynaptic compartment.

Collectively these data suggest that CAP2 is a postsynaptic protein relevant for shaping dendritic and spine morphology as well as for the regulation of synaptic transmission and plasticity, which are all deeply linked to the actin polymerization through cofilin activity (Hotulainen et al., 2009; Gu et al., 2010).

CAP2 forms disulfide-crosslinked dimers pivotal for association to cofilin and for actin turnover

The importance of protein self-association has been previously demonstrated for Srv2/CAP, the yeast homologous form of CAP2 (Hubberstey and Mottillo, 2002; Ono, 2013). Indeed, Srv2/CAP complex catalytically accelerates cofilin-dependent actin turnover (Balcer et al., 2003). The hexameric CAP molecules interact with the pointed ends of cofilin-decorated filaments promoting the disassembly (Chaudhry et al., 2013; Kotila et al., 2019; Shekhar et al., 2019). *In vitro* experiments have shown that the N-terminal domain of CAP2 forms tetramers have a high affinity for F-actin (Purde et al., 2019). Therefore, we wondered whether the mammalian CAP2 is also able to dimerize and oligomerize in a cellular system. Different experimental approaches were used to test this hypothesis. Either Myc-CAP2 or EGFP-CAP2 were transfected in COS-7 cells and we observed that both constructs are able to form aggregates in the cytoplasm, independently of the tag (Fig. 4A, lower panels). The transfection of both CAP2 constructs in COS-7 cells demonstrates that Myc-CAP2 and EGFP-CAP2 perfectly colocalize in cytoplasmic clusters, suggesting that CAP2 can self-associate (Fig. 4A). Coimmunoprecipitation assays performed from lysates of COS-7 cells cotransfected with Myc-CAP2 and

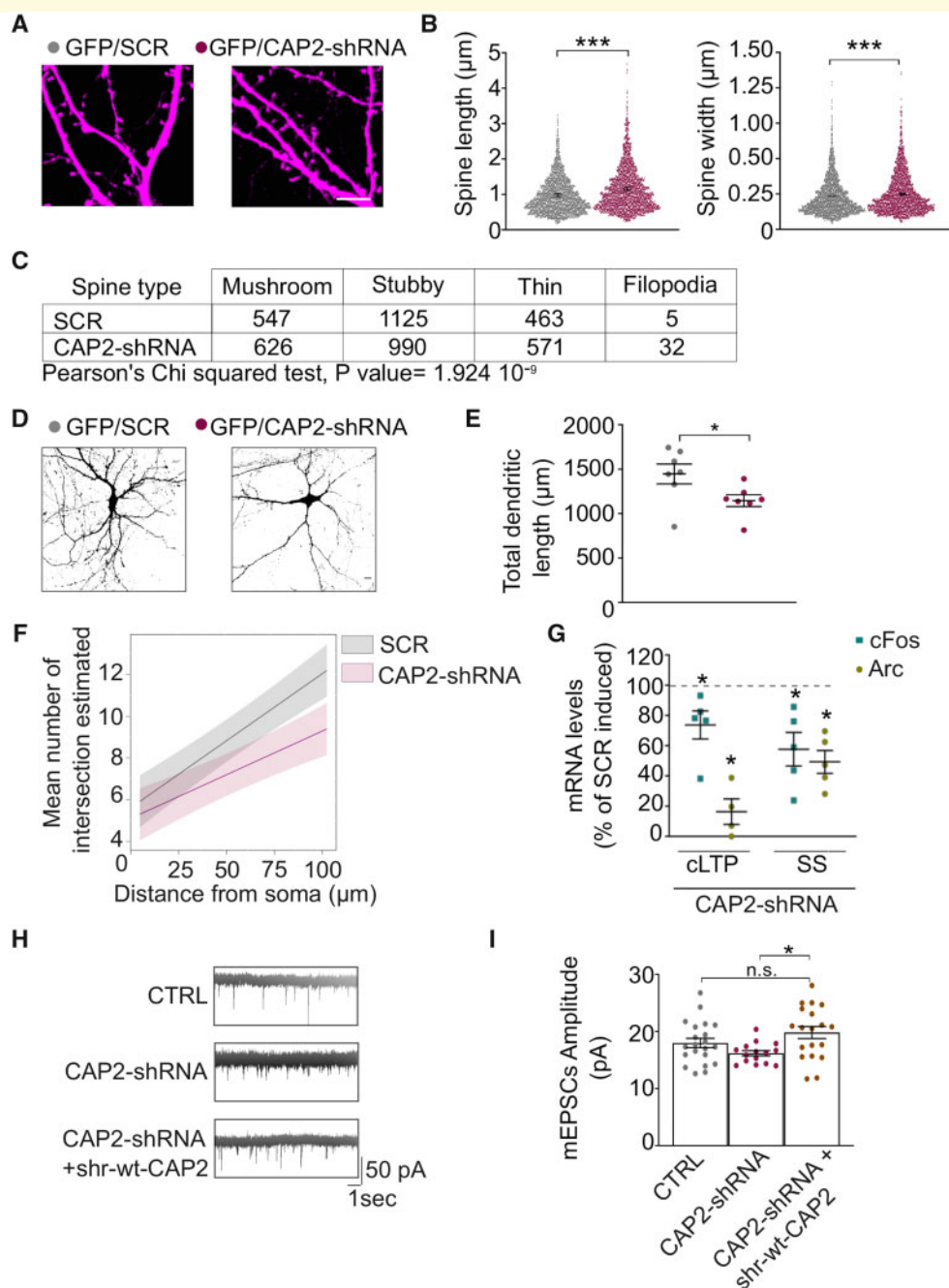


Figure 3 CAP2 is critical for neuronal structure and function. (A) Representative confocal images of primary hippocampal neurons transfected with GFP and either CAP2-shRNA or scramble sequence (SCR); scale bar = $5 \mu\text{m}$. (B) Graphs show the quantification of dendritic spine length and width (length, SCR = $0.956 \pm 0.061 \mu\text{m}$, CAP2-shRNA = $1.121 \pm 0.066 \mu\text{m}$; width, SCR = $0.4686 \pm 0.0097 \mu\text{m}$, CAP2-shRNA = $0.4998 \pm 0.0099 \mu\text{m}$, *t*-test from mixed-effects model: $***P < 0.001$, SCR $n = 2140$ spines, CAP2-shRNA $n = 2219$ spines). (C) The joint distribution of dendritic spine type and genetic modification is represented in the table together with the *P* value of the Chi-squared test of independence. (D) Representative micrographs of hippocampal neurons transfected with GFP and either CAP2-shRNA or SCR. Scale bar = $10 \mu\text{m}$. (E) Graph show the quantification of the total dendritic length (SCR = $1446.78 \pm 113.3 \mu\text{m}$, CAP2-shRNA = $1147.12 \pm 65.67 \mu\text{m}$, unpaired *t*-test from fixed-effects ordinary least squares regression model: $*P = 0.04995$, n SCR = 7 neurons, n CAP2-shRNA = 7 neurons). (F) The graph of Sholl analysis displays predicted values across available values of distance from soma (X axis) and corresponding 95% confidence bands (for details on how *P* values were calculated see Table 3, n SCR = 8 neurons, n CAP2-shRNA = 8 neurons). (G) QRT-PCR analysis of cFos and Arc expression in hippocampal neurons infected with either rAAV-CAP2-shRNA or rAAV-SCR and with or without treatment to induce either cLTP or synaptic stimulation (SS). The treated samples are normalized on either the cLTP-SCR or the SS-SCR condition. The down-regulation of CAP2 prevents the induction of Arc and cFos upon cLTP and SS (cLTP CAP2-shRNA versus cLTP-SCR, paired *t*-test: cFos $*P = 0.0485$, Arc $*P = 0.0137$; SS-CAP2-shRNA versus SS-SCR: cFos $*P = 0.0188$, Arc $*P = 0.003$, $n = 5$ independent experiments). (H) Representative traces of excitatory miniature postsynaptic currents (mEPSCs) recorded from 15 DIV hippocampal neurons obtained from CTRL, CAP2-shRNA and CAP2-shRNA+shr-wt-CAP2 transfected cultures. (I) Electrophysiological analysis of mEPSCs amplitude (pA): CTRL $n = 21$; CAP2 shRNA $n = 14$; CAP2 shRNA + shr-wt-CAP2 $n = 19$; one-Way ANOVA followed by Tukey's multiple comparison test: $*P = 0.013$, n.s. non-significant.

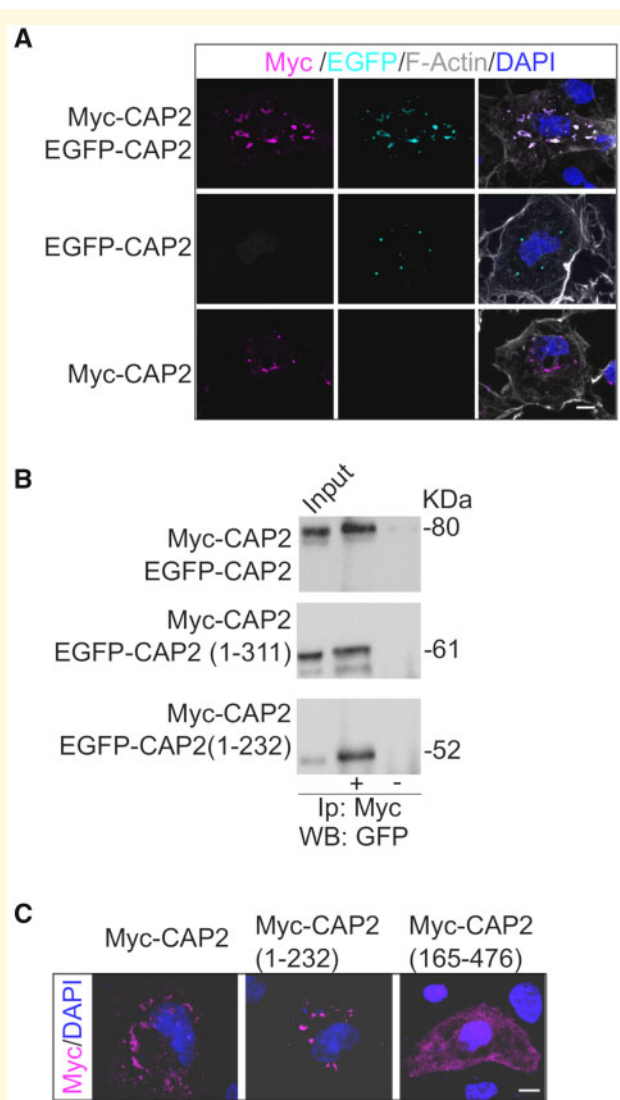


Figure 4 CAP2 self-associates. (A) Representative confocal images of COS-7 cells co-transfected with either Myc-CAP2 (magenta) or EGFP-CAP2 (cyan) or both constructs show the capability of CAP2 to form clusters. Scale bar = 10 μ m. (B) Homogenate of HEK293 cells transfected with Myc-CAP2 and either EGFP-CAP2 or EGFP-CAP2(1-232) or EGFP-CAP2(1-311) deletion mutants were immunoprecipitated (Ip) with anti-Myc antibody and the WB analysis carried out with anti-GFP antibody. The sequence 1-232 of CAP2 is sufficient for CAP2 self-association. Full uncropped blots are available in the [Supplementary material](#). (C) Representative confocal images of COS-7 cells transfected with Myc-CAP2, Myc-CAP2(1-232) and Myc-CAP2(165-476) reveal that the region 1-232 is sufficient for clusters formation while the deletion of the region 1-164 completely changes the protein intracellular pattern. Scale bar = 5 μ m.

EGFP-CAP2 confirmed that Myc-CAP2 interacts with EGFP-CAP2 (Fig. 4B).

The full three-dimensional (3D) structure of the human CAP2 is not available, but several studies have underlined the multi-domains organization of the protein (Ono, 2013). The only structural information that can be useful

to propose a possible 3D organization of the CAP2 dimer comes from the X-ray structure of the Helical Folded Domain (HFD) of the CAP homolog from *Dictyostelium discoideum* (Yusof et al., 2004). In details, this region is composed of an initial Coiled-coil region followed by a stable bundle of six antiparallel α -helices (HFD domain) (Supplementary Fig. 3A). This region (i.e. Coiled-coil and HFD) is not only conserved in CAP1 and CAP2 from human and mouse but also in the homologous CAP protein from *Dictyostelium discoideum* (Supplementary Fig. 3B). This evidence strengthens the idea that the dimerization/oligomerization of CAP2 is crucial for its cellular functions, such as the interaction with other protein partners (i.e. actin and cofilin).

To better characterize the region of CAP2 responsible for the self-association, we transfected COS-7 cells with Myc-CAP2 and either EGFP-CAP2 or the deletion mutant EGFP-CAP2(1-311) deleted of the CARP domain or the EGFP-CAP2(1-232) mutant lacking of the CARP domain, the proline rich sequences and the WH2 region (Peché et al., 2013) (Supplementary Fig. 3A). Coimmunoprecipitation experiments revealed that CAP2 self-association depends on its N-terminal region, similarly to what previously described for Srv2/CAP (Quintero-Monzon et al., 2009) (Fig. 4B). To investigate the involvement of N-terminus in CAP2-self-association, we performed imaging analysis in COS-7. The deletion mutant lacking the coiled-coil region and HFD, Myc-CAP2(165-476), displayed a diffuse staining throughout the cell, while Myc-CAP2 and Myc-CAP2(1-232) showed a clustered cytoplasmic distribution (Fig. 4C). In addition, coimmunoprecipitation assays confirmed that the deletion of the region 1-164 significantly reduces the self-association (Fig. 5A and B).

It has been recently demonstrated that CAP1 homodimerization depends on the formation of a disulfide bond that requires the Cys²⁹ of CAP1 (Liu et al., 2018). Therefore, we verified the presence of a disulfide cross-linked CAP2 dimer by loading an aliquot of hippocampal homogenate onto a non-reducing SDS-PAGE. As shown in Fig. 5C, both a band corresponding to CAP2 monomer at 58 kDa and a species of CAP2 with an apparent molecular weight of approximately double the CAP2 monomer (116 kDa) were detected. Importantly, the band corresponding to CAP2 dimer was eliminated by DTT, consistent with a disulfide cross-linked CAP2 dimer (Fig. 5C). To exclude the possibility that intra- and intermolecular disulfide bonds were non-specifically formed during the lysis process of the tissue, we carried-out the homogenization of rat hippocampus using a buffer containing iodoacetamide to protect free sulfhydryl groups. The samples were loaded onto a non-reducing SDS-PAGE and the WB analysis revealed the presence of both the CAP2 monomer and the CAP2 DTT-sensitive dimer (Supplementary Fig. 3C), thus confirming the existence of specific CAP2 disulfide cross-linked dimers in the hippocampus.

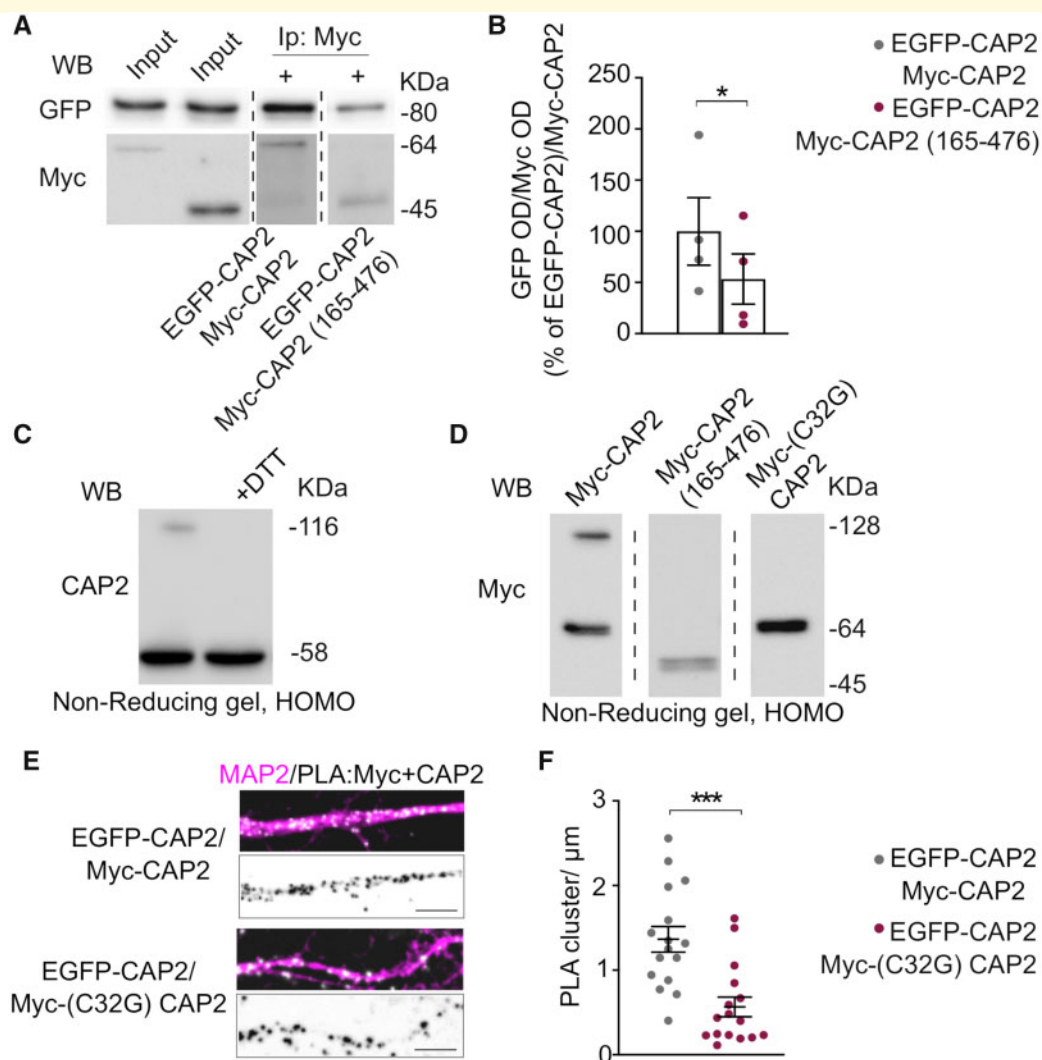


Figure 5 CAP2 forms dimers through Cys³². (A) Co-immunoprecipitation assays carried out from homogenate of HEK293 cells transfected with EGFP-CAP2 and either Myc-CAP2 or Myc-CAP2(165-476). The samples derive from the same experiment and gels/blots were processed in parallel. Full uncropped blots are available in the [Supplementary material](#). (B) The analysis of the optical density (OD) reveals that the lack of the sequence 1-164 of CAP2 significantly reduces CAP2 self-association [Myc-CAP2(165-476)/EGFP-CAP2 versus Myc-CAP2/EGFP-CAP2, paired *t*-test $P = 0.036$, $n = 4$ independent experiments]. (C) Representative WB of homogenates of rat brain hippocampus loaded onto a non-denaturing gel, without (left side) or with dithiothreitol (DTT) treatment (right side), as indicated. The band corresponding to the dimeric form of CAP2 is eliminated by DTT treatment. Full uncropped blots are available in the [supplementary material](#). (D) Representative WB of homogenates of HEK293 cells expressing Myc-CAP2, Myc-CAP2(165-476) or Myc-(C32G)CAP2. The deletion of the 1-164 region or the single point mutation Cys³² to Gly avoids the capability to form dimers. The samples derive from the same experiment and gels/blots were processed in parallel. Full uncropped blots are available in the [supplementary material](#). (E) Representative confocal images of PLA experiments showing proximity between EGFP-CAP2 and either Myc-CAP2 or Myc-(C32G)CAP2 (white) along MAP2 positive dendrites (magenta); lower panels, inverted images of PLA signal (black), scale bar = 5 μm. (F) Graphs show the quantification of the PLA clusters/μm (EGFP-CAP2/Myc-CAP2 = 1.366 ± 0.150 , EGFP-CAP2/Myc-(C32G)CAP2 = 0.566 ± 0.117 , *t*-test from mixed-effects model: *** $P < 0.0001$; n EGFP-CAP2/Myc-CAP2 = 16 neurons, n EGFP-CAP2/Myc-(C32G)CAP2 = 16 neurons).

To identify the region of CAP2 responsible for dimerization, we transfected COS-7 cells with either Myc-CAP2 or a deletion mutant lacking of the N-terminal region [Myc-CAP2(165-476)] and the lysates were loaded onto a non-reducing SDS-PAGE. As shown in [Fig.5D](#), CAP2 monomer and dimer were detectable when Myc-CAP2 was expressed, while the deletion of the N-terminal

region [Myc-CAP2(165-476)] abolishes the CAP2 capability to form dimers, demonstrating that this is the domain involved in the dimerization. Interestingly, only one Cys residue is present in the CAP2 region spanning from amino acid 1 to 164. Notably, the Myc-CAP2 mutant carrying the mutation of the Cys³² to Gly [Myc-(C32G)CAP2] is not able to dimerize in non-reducing

SDS-PAGE (Fig. 5D). To strengthen these data, we performed a PLA in hippocampal neurons transfected with EGFP-CAP2 and either Myc-CAP2 or Myc-(C32G)CAP2. In neurons expressing EGFP-CAP2 and Myc-CAP2, a large number of PLA signals were detected when the two antibodies anti-GFP and anti-Myc were used, indicating that these two CAP2 constructs are in close proximity to each other along MAP2-positive dendrites (Fig. 5E). In neurons transfected with EGFP-CAP2 and the mutant Myc-(C32G)CAP2, the density of PLA signals significantly decreased when compared to cells overexpressing EGFP-CAP2 and Myc-CAP2 (Fig. 5F). For control experiments, only the anti-Myc primary antibody was used and no PLA signal was generated (Supplementary Fig. 3D). Overall, these findings suggest that the Cys³² is fundamental for the formation of CAP2 dimers and for CAP2 clustering in neurons.

To investigate the direct effect of monomeric and dimeric CAP2 on the assembly and stability of individual actin filaments, we employed *in vitro* dual-colour total internal reflection fluorescence microscopy. *In vitro* polymerization of a mixture of unconjugated and Alexa-Fluor-561-conjugated actin occurs spontaneously at certain actin concentrations until it reaches equilibrium of G- and F-actin. We then added the purified recombinant CAP2 and (C32G)CAP2 proteins and determined the rate of F-actin depolymerization caused by G-actin washout, using kymograph analysis. The data showed a clear increase of actin depolymerization in the presence of CAP2 that was prevented by the mutation of Cys³² to glycine (Fig. 6A and B). In addition, the analysis of the filaments showed that the CAP2-dependent increase in actin depolymerization rate was related to an increase in the severing activity (Fig. 6C and D). Non-reducing SDS-PAGE assays of the recombinant proteins confirmed that CAP2, but not the mutant (C32G)CAP2, forms dimers (Supplementary Fig. 4A). Remarkably, WB analysis revealed that cofilin was co-purified with CAP2, but in a smaller extent with the mutant (C32G)CAP2 (Fig. 6E).

To confirm that the lack of Cys³² affects CAP2 association with cofilin, PLA assays were performed in primary hippocampal neurons transfected with either Myc-CAP2 or Myc-(C32G)CAP2. The analysis of the PLA signals confirms a significant decrease in the association between Myc-(C32G)CAP2 and cofilin when compared to the binding of Myc-CAP2 to cofilin (Fig. 6F and G). For control experiments, when anti-Myc primary antibody or anti-cofilin antibody alone was used, no PLA signal was generated (Supplementary Fig. 4B). As control, we verified that the association of CAP2 with actin was not affected by the mutation of the Cys³² to Gly (Supplementary Fig. 4C). Therefore, the lack of the disulfide bond involving CAP2 Cys³² abolishes the CAP2 dimerization, reduces the cofilin binding and, thereby, prevents the increase in actin depolymerization rate in total internal reflection fluorescence microscopy experiments.

Long-term potentiation triggers CAP2 dimer formation as a crucial step for structural plasticity

Given the key role of cofilin-mediated actin dynamics in the structural remodelling of spines during activity-dependent synaptic plasticity phenomena (Bosch *et al.*, 2014), we tested whether either LTP or LTD could modulate CAP2 dimerization, and consequently its association with cofilin.

First, we investigated CAP2 homodimer localization in the postsynaptic compartment. WB analyses showed that CAP2 dimer levels are higher in the postsynaptic TIF compared to the total homogenate (Supplementary Fig. 5A) in both rat and human hippocampus, thus confirming the existence of CAP2 dimer in human and revealing the enrichment of the CAP2 dimer in this subcellular compartment.

Second, we asked whether LTP regulates CAP2 synaptic availability in the dendritic spines. To this, we induced cLTP in hippocampal cultures that results in prolonged NMDA receptor-dependent LTP (Marcello *et al.*, 2013). Thirty minutes after cLTP induction, we purified TIF from control and cLTP-treated hippocampal neurons. WB analysis revealed that cLTP elicited an increase in the CAP2 levels in the TIF fraction compared to control neurons, without affecting the total levels of the protein (Fig. 7A and B). Notably, cLTP stimulation caused also a significant increase in CAP2 dimer levels in TIF (Fig. 7C and D). Secondly, to evaluate whether these effects could be ascribed to the CAP2 Cys³²-dependent dimerization, we analysed the PLA signal upon cLTP induction in hippocampal neurons transfected with EGFP-CAP2 and either Myc-CAP2 or Myc-(C32G)CAP2. The cLTP induction significantly increased the PLA signal in neurons transfected with EGFP-CAP2 and Myc-CAP2, confirming the LTP-triggered augment in CAP2 self-association. On the other hand, no modifications in PLA signals upon LTP induction were detected when EGFP-CAP2 and Myc-(C32G)CAP2 were expressed (Fig. 7E and F). This effect is specifically related to LTP, since both PLA and WB analysis of the synaptic fraction revealed no variations in CAP2 synaptic levels and in dimer formation after cLTD induction (Supplementary Fig. 5E–G).

To determine if the increase in LTP-driven CAP2 dimer formation affects the association with cofilin, we performed PLA assays after cLTP induction in neurons transfected with either Myc-CAP2 or Myc-(C32G)CAP2. As shown in Fig. 7G and H, LTP fosters the association of cofilin with CAP2. Likewise, we detected a significant increase in the association between endogenous CAP2 and cofilin upon LTP induction, indicating that this effect was not related to the overexpression of Myc-CAP2 construct (Supplementary Fig. 5H). The Cys³²-dependent self-association of CAP2 is required because the Myc-

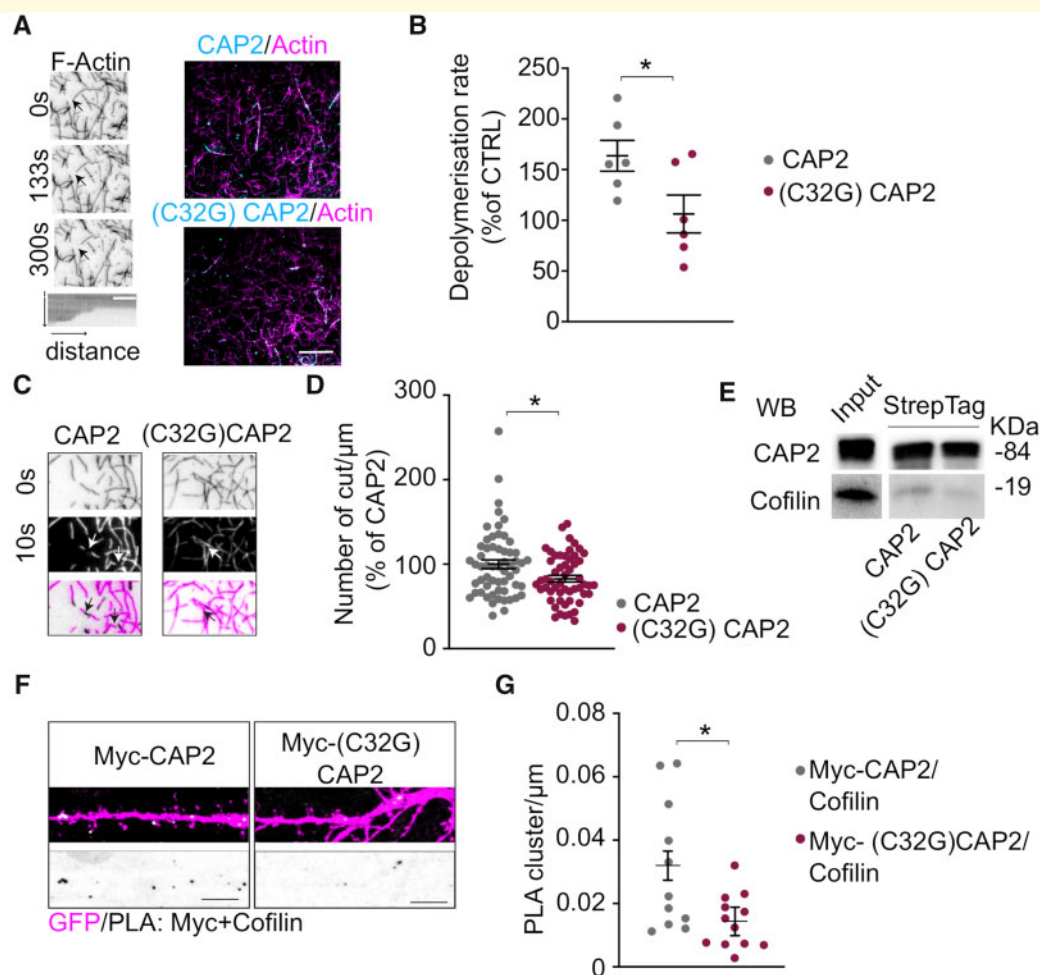


Figure 6 Cys³²-dependent CAP2 dimerization is relevant for association with cofilin and for controlling actin depolymerization. (A) Spontaneous *in vitro* depolymerization of F-actin-Alexa Fluor 568 visualized by total internal reflection fluorescence microscopy. Left panels, actin filament undergoing depolymerization upon G-actin wash-out, arrowheads indicate the barbed ends of the filament. Right panels, overlay images show the actin filaments (magenta) and either CAP2 or (C32G)CAP2 mutant (cyan). Scale bar = 5 μ m. (B) Kymographs analysis of F-actin depolymerization rate indicates that CAP2 increases the depolymerization rate of F-actin while the mutant (C32G)CAP2 abolished this effect [(C32G)CAP2 versus CAP2, unpaired *t*-test: $*P = 0.038$, $n = 6$ independent experiments]. (C) Representative images of the analysis of the severing activity show an actin filament undergoing depolymerization in presence of either CAP2 or (C32G)CAP2 and arrowheads indicate the presence of cutting sites. (D) The number of cuts/ μ m significantly decreases in presence of (C32G)CAP2 compared to CAP2 [(C32G)CAP2 versus CAP2, unpaired *t*-test: $*P = 0.01$, n (C32G)CAP2 = 54 filaments, n CAP2 = 58 filaments]. (E) WB of the Streptag CAP2 and (C32G)CAP2 fusion proteins shows that the mutation of C32 to G reduces CAP2 capability to bind cofilin. Full uncropped blots are available in the [supplementary material](#). (F) Images showing PLA signal between cofilin and either Myc-CAP2 or Myc-(C32G)CAP2 (white) along MAP2 positive dendrites (magenta). Scale bar = 5 μ m. Lower panels, inverted images of PLA signal (black). (G) The mutation of Cys³² significantly reduces association with cofilin, as shown in the graphs reporting the quantification of the PLA clusters/ μ m (Myc-CAP2 = 0.0320 ± 0.005 ; Myc-(C32G)CAP2 = 0.0144 ± 0.005 , unpaired *t*-test from fixed-effects ordinary least squares regression model: $*P = 0.0146$, Myc-CAP2 $n = 11$ neurons, Myc-(C32G)CAP2 $n = 12$ neurons).

(C32G)CAP2 mutant prevents the LTP-induced increase in CAP2/cofilin interaction (Fig. 7G and H).

Overall, these findings suggest that LTP triggers CAP2 translocation to the spine and the formation of Cys³²-dependent dimers, thus promoting the association of CAP2 with cofilin.

In the initial phase of LTP, the actin cytoskeleton is rapidly remodelled while active cofilin is transported to the spine (Bosch *et al.*, 2014). In light of this observation,

we attempted to determine whether the hampering CAP2 dimerization impairs LTP-driven enrichment of cofilin in the spine. To this, we induced cLTP in primary hippocampal neurons transfected with either CAP2-shRNA or the corresponding control scramble sequence. These constructs express the fluorescent protein mCherry under the control of the neuron-specific Ca²⁺/calmodulin-dependent protein kinase II promoter. To assess the magnitude of accumulation, we took advantage of structured

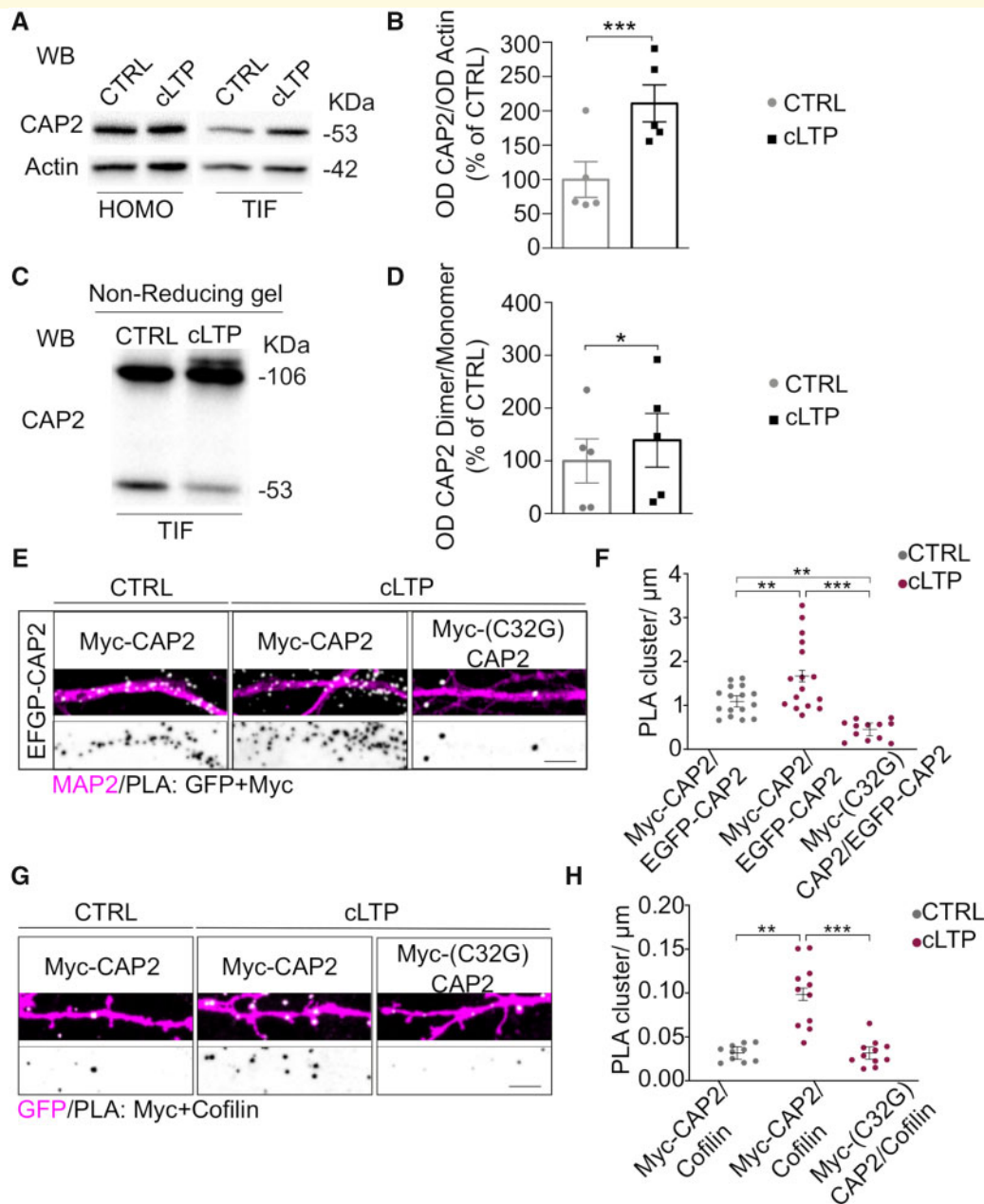


Figure 7 LTP promotes CAP2 synaptic localization, dimer formation and association with cofilin. **(A)** Representative WB of CAP2 and actin in Homo and TIF samples obtained from control and cLTP-treated neurons, 30 min after the cLTP induction. Non-cropped blots are shown in [Supplementary Fig. 5B and C](#). **(B)** cLTP promotes CAP2 enrichment in the TIF (cLTP versus CTRL, paired *t*-test: $***P = 0.0008$, $n = 5$ independent experiments). **(C)** Representative WB of CAP2 dimer and monomer in TIF samples obtained from control and cLTP-treated neurons, 30 min after the cLTP induction. Non-cropped blots are shown in [Supplementary Fig. 5D](#). **(D)** cLTP increases CAP2 dimer/monomer ratio in the TIF fraction of cLTP-treated neurons (cLTP versus CTRL, paired *t*-test: $*P = 0.042$, $n = 5$ independent experiments). **(E)** PLA representative images showing the proximity between EGFP-CAP2 and either Myc-CAP2 or Myc-(C32G)CAP2 (white) along MAP2 positive dendrites (magenta) 30 min after cLTP induction. Lower panels, inverted images of PLA signal (black), scale bar = 5 μm . **(F)** Graphs show the quantification of the PLA clusters/ μm (EGFP-CAP2/Myc-CAP2-CTRL = 1.100 ± 0.128 , EGFP-CAP2/Myc-CAP2-cLTP = 1.679 ± 0.128 , EGFP-CAP2/Myc-(C32G)CAP2-cLTP = 0.461 ± 0.148 , linear mixed-effects model, false discovery rate adjustment for multiple comparisons for the contrasts of interest: $**P = 0.00129$, $***P < 0.0001$, *P* values for all the multiple comparisons are reported in [Table 4](#); EGFP-CAP2/Myc-CAP2-CTRL $n = 16$ neurons, EGFP-CAP2/Myc-CAP2-cLTP $n = 16$ neurons, EGFP-CAP2/Myc-(C32G)CAP2-cLTP $n = 12$ neurons). **(G)** PLA images revealing the closeness between cofilin and either Myc-CAP2 or Myc-(C32G)CAP2 (white) along dendrites of GFP transfected hippocampal neurons (magenta) after cLTP induction. Lower panels, inverted images of PLA signal (black), scale bar = 5 μm . **(H)** Graphs show the quantification of the PLA clusters/ μm (MycCAP2/cofilin-CTRL = 0.0317 ± 0.0073 , MycCAP2/cofilin-cLTP = 0.0984 ± 0.0070 , Myc-(C32G)-CAP2/cofilin-cLTP = 0.0315 ± 0.0070 , linear mixed-effects model, false discovery rate adjustment for multiple comparisons for the contrasts of interest: $***P < 0.0001$, *P* values for all the multiple comparisons are reported in [Table 4](#); MycCAP2/cofilin-CTRL $n = 10$ neurons, MycCAP2/cofilin-cLTP $n = 11$ neurons, Myc-(C32G)CAP2/cofilin-cLTP $n = 11$ neurons).

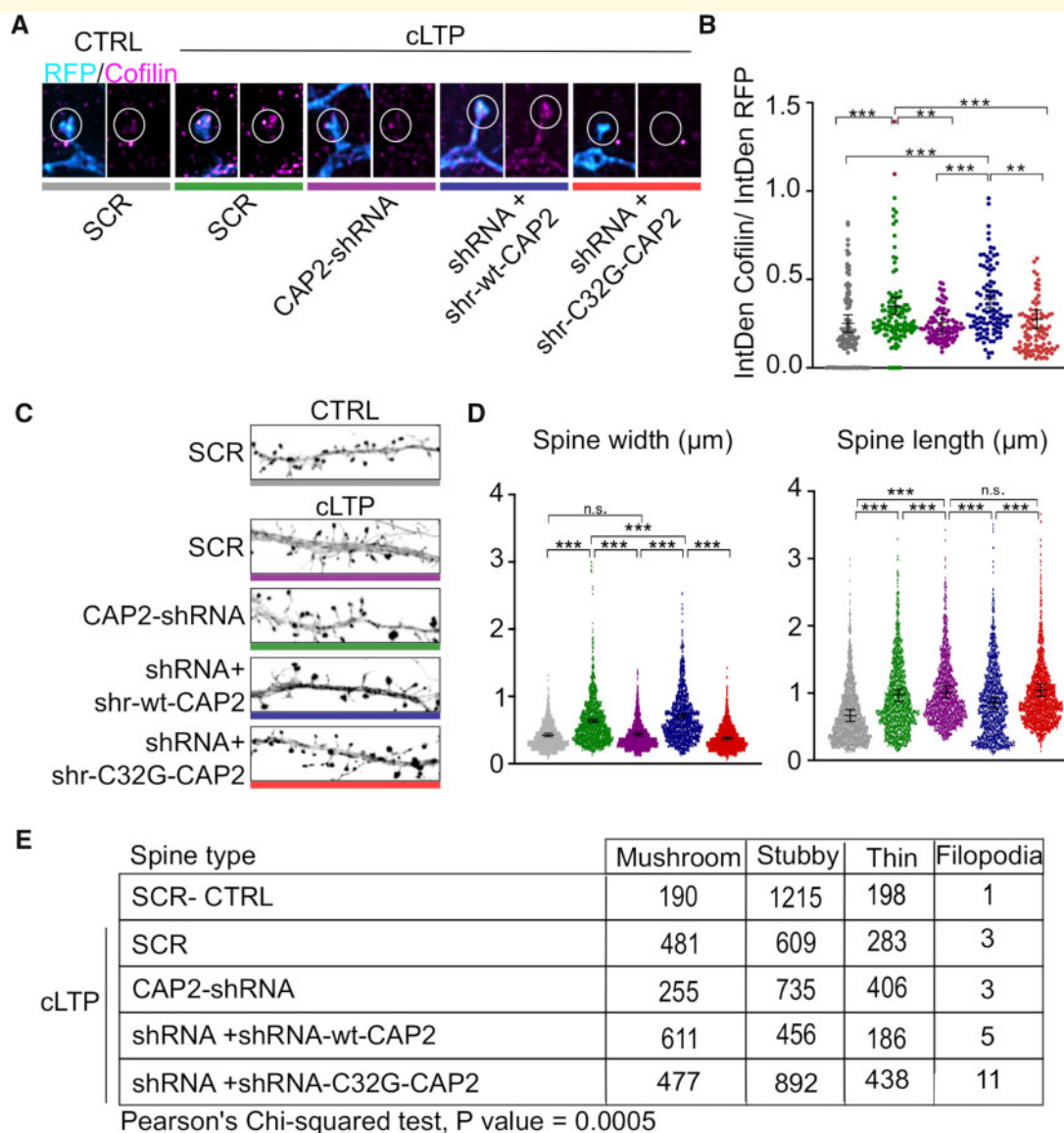


Figure 8 Cys³²-dependent CAP2 dimer is required for cofilin translocation and for structural plasticity changes. **(A)** Structured illumination microscopy images of cofilin (magenta) and RFP (cyan) staining of primary hippocampal neurons transfected with vectors expressing RFP and either scramble sequence (SCR) or CAP2-shRNA or CAP2-shRNA + shr-wt-CAP2 or CAP2-shRNA + shr-C32G-CAP2, 30 min after cLTP induction. Scale bar = 2 μ m. **(B)** Graphs show the quantification of the ratio between the integrated density (IntDen) of cofilin and RFP staining in dendritic spines (SCR-CTRL = 0.257 ± 0.049 , SCR-cLTP = 0.357 ± 0.049 , CAP2-shRNA-cLTP = 0.263 ± 0.050 , CAP2-shRNA + shr-wt-CAP2-cLTP = 0.396 ± 0.050 , CAP2-shRNA + shr-C32G-CAP2-cLTP = 0.282 ± 0.050 , linear mixed-effects model, false discovery rate adjustment for multiple comparisons for the contrasts of interest: *** $P < 0.0001$; ** $P < 0.001$, SCR-CTRL $n = 107$ spines, SCR-cLTP $n = 120$ spines, CAP2-shRNA-cLTP $n = 94$ spines, CAP2-shRNA + shr-wt-CAP2-cLTP $n = 104$ spines, CAP2-shRNA + shr-C32G-CAP2-cLTP $n = 96$ spines). **(C)** Confocal images of RFP staining of primary hippocampal neurons transfected with vectors expressing RFP and either SCR or CAP2-shRNA or CAP2-shRNA + shr-wt-CAP2 or CAP2-shRNA + shr-C32G-CAP2, 30 min after cLTP induction; scale bar = 5 μ m. **(D)** Graphs show the quantification of dendritic spine head length and width (length, SCR-CTRL = 0.672 ± 0.089 μ m, SCR-cLTP = 0.971 ± 0.089 μ m, CAP2-shRNA-cLTP = 1.019 ± 0.089 μ m, CAP2-shRNA + shr-wt-CAP2-cLTP = 0.860 ± 0.089 μ m, CAP2-shRNA + shr-C32G-CAP2-cLTP = 1.039 ± 0.089 μ m; width, SCR-CTRL = 0.428 ± 0.026 μ m, SCR-cLTP = 0.638 ± 0.026 μ m, CAP2-shRNA-cLTP = 0.440 ± 0.026 μ m, CAP2-shRNA + shr-wt-CAP2-cLTP = 0.711 ± 0.026 μ m, CAP2-shRNA + shr-C32G-CAP2-cLTP = 0.381 ± 0.026 μ m; linear mixed-effects model, false discovery rate adjustment for multiple comparisons for the contrasts of interest: *** $P < 0.0001$, n.s. non significant, P values for all the multiple comparisons are reported in Table 4; SCR-CTRL $n = 1604$ spines, SCR-cLTP $n = 1376$ spines, CAP2-shRNA-cLTP $n = 1399$ spines, CAP2-shRNA + shr-wt-CAP2-cLTP $n = 1258$ spines, CAP2-shRNA + shr-(C32G)-CAP2-cLTP $n = 1818$ spines). **(E)** The joint distribution of dendritic spine type and the combination of genetic modification/treatment is represented in the table together with the P value of the Chi-squared test of independence.

illumination microscopy to calculate the relative concentration of cofilin in the spine by dividing cofilin intensity by mCherry intensity (Bosch *et al.*, 2014). As previously demonstrated (Bosch *et al.*, 2014), after 30 min from cLTP induction, cofilin is highly enriched in the spines of neurons transfected with the scramble sequence, while the down-regulation of CAP2 prevents the LTP-triggered translocation of cofilin in the spine. To assess whether this effect could be specifically ascribed to CAP2 and to determine the role of the Cys³², we used shr-wt-CAP2 as a rescue and we generated and validated the mutant shr-C32G-CAP2 that was insensitive to the CAP2-shRNA (Supplementary Fig. 5I). Importantly, the transfection of the shRNA-resistant CAP2 construct (shr-wt-CAP2), but not the expression of shr-C32G-CAP2, restores the LTP-driven translocation of cofilin to the spines (Fig. 8A and B). These data demonstrate that CAP2 and the Cys³²-dependent dimerization of the protein are essential for the LTP-triggered cofilin trafficking to spines.

Since cofilin translocation to spines during LTP is required for actin cytoskeleton dynamics and spine enlargement, we verified whether the loss of Cys³² and, thereby, of CAP2 dimerization impairs LTP-induced spine remodelling. An accurate analysis of dendritic spine morphology demonstrated that cLTP induces the expected spine head enlargement in control conditions, but not in neurons transfected with CAP2-shRNA (Fig. 8C and D). cLTP triggers a significant increase in spine length that is not restored to control levels by CAP2 down-regulation (Fig. 8C and D). The expression of the shr-wt-CAP2, but not of the mutant shr-C32G-CAP2, slightly potentiates the LTP-induced increase in spine head width (Fig. 8C and D). Regarding the spine length, the mutant shr-C32G-CAP2 does not rescue the effect of CAP2 down-

regulation in cLTP-treated neurons, while shr-wt-CAP2 expression reduces the cLTP-triggered increase in spine length (Fig. 8C and D). The analysis of the different spines categories revealed the presence of a significant association between spines populations and the combination of cLTP treatment and manipulation of CAP2 expression (Fig. 8E), showing the importance of CAP2 in LTP-triggered modifications in spine morphology.

Furthermore, taking advantage of electrophysiological recordings of mEPSCs, we addressed the functional impact of CAP2 down-regulation on hippocampal plasticity by induction of cLTP. As indicated in Fig. 9A and B, cLTP mediates a significant increment in mEPSCs amplitude of excitatory synaptic events only in control cultures whereas no potentiation occurs in CAP2-shRNA neurons. Similarly, cultures transfected with the shr-C32G-CAP2 mutants do not display any potentiation that is rescued only in the shRNA+shr-wt-CAP2 control group (Fig. 9A and B). Taken together, these results suggest that synaptic plasticity is affected by CAP2 and that mutation in the residue Cys³² is sufficient for defective CAP2 activity and LTP induction.

CAP2 dimer association with cofilin is altered in Alzheimer's disease

Since Cys³²-dependent CAP2 homodimerization is crucial for the regulation of dendritic spine morphology and synaptic plasticity via cofilin binding, we wondered whether alterations of this mechanism were detectable in Alzheimer's disease synapses, where we found an aberrant increased level of cofilin along with a significant reduction in CAP2 (Fig. 1).

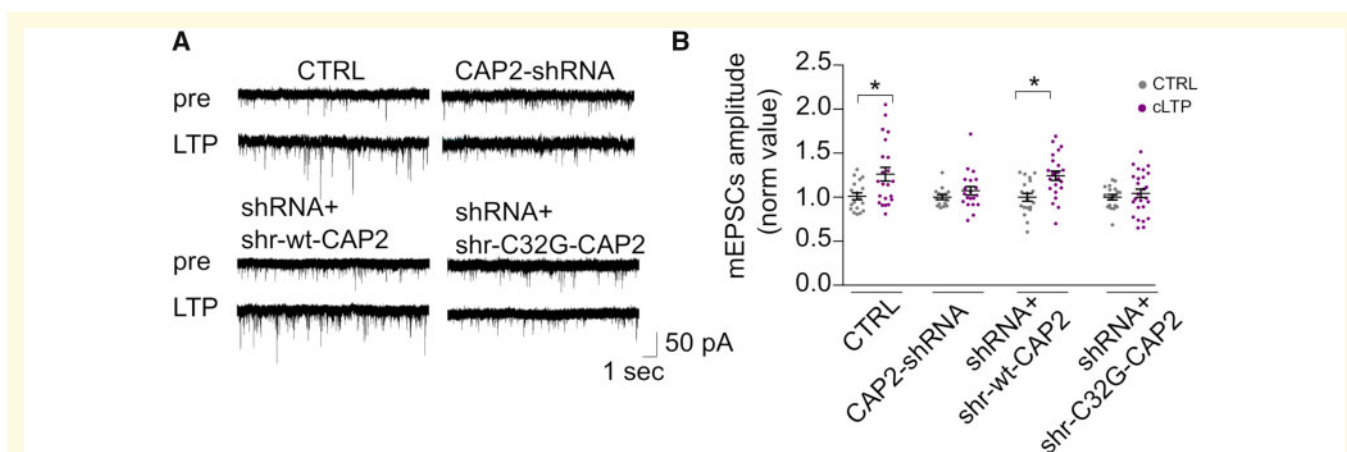


Figure 9 Cys³²-dependent CAP2 dimer is relevant for synaptic transmission potentiation upon LTP induction.

(A) Electrophysiological recordings of mEPSCs before and after chemical LTP (cLTP) induction in 15 DIV hippocampal neurons. Representative mEPSC traces. (B) Differently from CTRL and shr-wt-CAP2 cells, CAP2-shRNA and CAP2-shRNA+shr-C32G-CAP2 neurons are unable to undergo cLTP. mEPSCs amplitude (normalized values): CTRL = 1 ± 0.03 ($n = 18$) versus cLTP: 1.26 ± 0.07 ($n = 22$); CAP2-shRNA: 1 ± 0.02 ($n = 15$) versus cLTP: 1 ± 0.02 ($n = 20$); shRNA+shr-wt-CAP2: 1 ± 0.04 ($n = 19$) versus cLTP: 1.25 ± 0.05 ($n = 23$); shRNA+shr-C32G-CAP2: 1 ± 0.031 ($n = 18$) versus cLTP: 1 ± 0.04 ($n = 26$). One-way ANOVA, Holm-Sidak's multiple comparisons test: $P < 0.0001$.

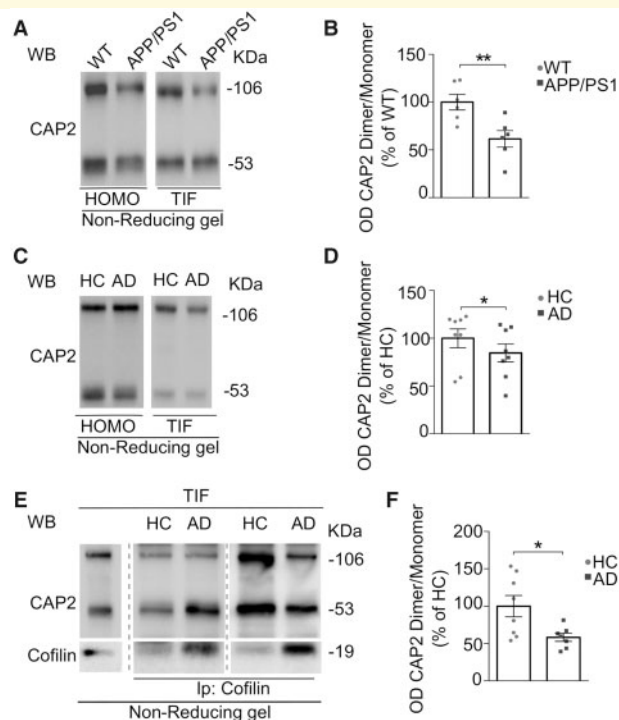


Figure 10 Cys³²-dependent CAP2 dimer levels and CAP2 association to cofilin are affected in Alzheimer's disease synapses.

(A) Representative WB of CAP2 dimer level in the HOMO and TIF hippocampal fraction of APP/PS1 and WT animals. Full uncropped blots are available in the [supplementary material](#). (B) Quantitative analysis shows the decreased ratio of CAP2 dimer OD on the CAP2 monomer OD of APP/PS1 mice compared to WT (TIF, APP/PS1 versus WT, paired *t*-test: $*P = 0.003$, n WT = 6 mice, n APP/PS1 = 6 mice). (C) Representative WB showing the levels of CAP2 monomer and dimer in the HOMO and TIF samples of Alzheimer's disease (AD) and HC hippocampal samples. Full uncropped blots are available in the [Supplementary material](#). (D) Quantitative analysis shows that CAP2 dimer/monomer ratio is reduced in AD patients TIF but not in HOMO (TIF, AD versus HC paired *t*-test: $*P = 0.014$, n HC = 8, n AD = 8). (E) TIF from hippocampi of HC and AD patients were immunoprecipitated (ip) with anti-cofilin antibody and CAP2 coprecipitation evaluated in non-denaturing condition. Samples derive from the same experiment and gels/blots were processed in parallel. Full uncropped blots are available in the [Supplementary material](#). (F) Cofilin binding to CAP2 is altered in TIF fraction of AD compared with HC (CAP2 dimer/monomer, AD versus HC, unpaired *t*-test: $*P = 0.023$, n HC = 8, n AD = 7).

The analysis of the CAP2 dimer/monomer ratio in APP/PS1 and WT mice hippocampi revealed a significant decrease of dimer levels in the postsynaptic fraction, but not in the total homogenate, of APP/PS1 mice when compared to WT mice (Fig. 10A and B, [Supplementary Fig. 6A](#)). We examined the CAP2 homodimer formation in Alzheimer's disease patients' hippocampi and the quantitative results showed a significant reduction in CAP2 dimer/monomer ratio specifically in the synapse of Alzheimer's disease patients compared to HC, while no changes were detected in the total homogenate (Fig. 10C and D, [Supplementary Fig. 6B](#)).

Since CAP2 dimer formation is relevant for CAP2 association with cofilin and for cofilin localization in the postsynaptic compartment, we verified whether cofilin binding to CAP2 monomer and dimer is affected in Alzheimer's disease. Given that cofilin is aberrantly increased in the Alzheimer's disease hippocampi postsynapse, we focused on TIF samples obtained from HC and Alzheimer's disease patients. TIF samples were

immunoprecipitated with cofilin antibody and loaded onto a non-reducing gel. WB analysis carried out with a CAP2 antibody revealed that cofilin specifically precipitates both CAP2 monomer and dimer in human postsynaptic compartment ([Supplementary Fig. 6C](#)), confirming CAP2 dimer and monomer as binding partners of cofilin in human. The quantitative analysis of coimmunoprecipitation experiments revealed that the ratio of CAP2 dimer/monomer bound to cofilin is significantly reduced in Alzheimer's Disease patients when compared to HC (Fig. 10E and F; [Supplementary Fig. 6D](#)), that is in line with the availability of the CAP2 dimer/monomer in the postsynaptic compartment.

In light of the above, we tested whether the association between single nucleotide polymorphisms of CAP2 Cys³² (rs750613178 variant) and Alzheimer's disease onset might occur. To this aim, a preliminary screening experiment of genetic polymorphism has been performed on 70 Alzheimer's disease patients (age = 68.2 ± 16.3 ; female% = 76.8). No genetic variations of CAP2 Cys³² were

detected in Alzheimer's disease patients, suggesting that other cellular mechanisms might be responsible for the decreased synaptic dimer levels in Alzheimer's disease.

Discussion

A major question in Alzheimer's disease pathogenesis is to define the mechanism guiding alteration of synaptic plasticity and spine dysmorphogenesis. Here, we show that CAP2 is able to control cofilin synaptic availability during activity-dependent plasticity phenomena. Remarkably, this mechanism is specifically altered in the hippocampus of Alzheimer's disease patients and of an Alzheimer's disease mouse model.

CAP2 has been reported as a multi-domain actin binding protein, expressed in specific tissues, including the brain (Peche et al., 2007; Kumar et al., 2016). Our study provides a detailed characterization of CAP2 in neurons bringing into focus conclusive evidences for both CAP2 localization in the postsynaptic compartment and its pivotal role in synaptic plasticity phenomena. This has been demonstrated with different approaches. First, stimulated emission depletion nanoscopy and biochemical fractionation approaches showed that CAP2 is localized in the postsynaptic compartment, in the region just underneath the PSD where F-actin is enriched (Korobova and Svitkina, 2010). Secondly, we observed that the down-regulation of CAP2 impairs neuronal architecture and spine shape, together with a decrease in synaptic excitatory transmission. Such alterations are translated into an impairment of plasticity phenomena.

Furthermore, the down-regulation of CAP2 decreases the levels of BDNF, a neurotrophin important for neuronal survival and synaptic plasticity (Lynch et al., 2008) and reduced early in the course of the disease (Kaminari et al., 2017). Its delivery could rescue memory deficits dendrite outgrowth and spine loss (de Pins et al., 2019). Therefore, we can hypothesize a role for CAP2 in the alterations of BDNF in Alzheimer's disease and in the consequent impairment of plasticity phenomena.

It has been shown that CAPs and cofilin synergize to depolymerize actin filaments (Chaudhry et al., 2013; Kotila et al., 2019; Shekhar et al., 2019), highlighting the critical role of this protein family in actin-dependent processes. In line with these results, total internal reflection fluorescence experiments showed that CAP2 increases the actin depolymerization rate. Considering that an efficient actin turnover in spines is required for functional LTP (Okamoto et al., 2004), we observed that the down-regulation of CAP2 leads to the lack of both potentiation and spine head enlargement expected upon cLTP induction.

Why is CAP2 critical for plasticity phenomena? CAP2 has been reported as a binding partner of cofilin (Kumar et al., 2016), a master regulator of postsynaptic actin dynamics and structural plasticity (Rust, 2015a). Upon LTP

induction, cofilin activity is first increased and subsequently decreased, allowing first for actin remodelling and then for an increase in F-actin and associated spine enlargement (Fukazawa et al., 2003; Chen et al., 2007; Gu et al., 2010). Even though cofilin phosphorylation is considered one of the major mechanisms controlling its activity (Van Troys et al., 2008; Bernstein and Bamburg, 2010; Rust, 2015a), the regulation of its availability and retention in spines could also contribute to cofilin-dependent sculpturing of the cytoskeleton. Cofilin indeed accumulates in regions of the spine that contain a dynamic F-actin network responsible for spine morphological changes during synaptic plasticity (Racz and Weinberg, 2006). Importantly, cofilin is translocated to the spine upon LTP induction (Bosch et al., 2014) and our findings show that CAP2 down-regulation blocks the LTP-triggered enrichment of cofilin in spines. The impaired cofilin localization in spines and, thereby, the defects in structural and functional synaptic plasticity could be rescued by cotransfection of the cells with an shRNA-resistant CAP2 construct, confirming that the described CAP2-knockdown phenotypes indeed resulted from diminished CAP2 expression.

Furthermore, we also addressed the key question regarding the molecular determinants relevant for CAP2/cofilin association. A careful mapping of CAP2 structure was carried out and, by using different approaches, we showed that the N-terminal domain of CAP2 is responsible for its self-association, as previously demonstrated for Svr2/CAP protein (Quintero-Monzon et al., 2009). In particular, in this region we identified the Cys³² as the amino acid involved in the formation of disulfide cross-linked CAP2 dimers. The mutation of Cys³² to Gly dramatically reduces, but not completely abolishes, CAP2 self-association and the binding to cofilin, suggesting that CAP2 can still form aggregates capable of interacting with cofilin. However, the lack of Cys³²-dependent CAP2 homodimer results in a loss of function of CAP2/cofilin complex on actin depolymerization, highlighting the importance of such disulfide bond for the operational role of CAP2. In fact, the CAP2 construct carrying the mutation Cys³² to Gly significantly attenuates the capability of CAP2 of promoting actin filaments depolymerization in an *in vitro* assay. A similar molecular pathway has been shown for CAP1, since Cys²⁹-dependent homodimerization of CAP1 affects binding to cofilin and F-actin stability (Liu et al., 2018). Notably, the Cys²⁹ residue of CAP1 is not conserved in human, thus limiting the relevance of CAP1-dependent mechanism and highlighting the role of CAP2 as main regulator of cofilin in human neuronal cells.

To strengthen the critical role of CAP2 homodimer in the spine, we show that it is localized in the postsynaptic compartment and it undergoes a dynamic regulation of its synaptic levels by activity-dependent synaptic plasticity. The LTP-induced increase in CAP2 localization in spines promotes the formation of CAP2 dimers through

Cys³², and thereby fosters CAP2 association with cofilin. This event is required for LTP-induced translocation of cofilin to the spine and for structural changes and the potentiation of synaptic transmission underlying LTP expression. Indeed, the WT CAP2 construct, but not the CAP2 mutant carrying the Cys³² mutated to Gly, restores and slightly increases the LTP-triggered enlargement of spine head in CAP2-knockdown neurons. In addition, the structured illumination microscopy analysis of cofilin localization in spines revealed that the CAP2 mutant failed to rescue the expected enrichment of cofilin in spines upon LTP. These data suggest that the increased synaptic availability of CAP2 monomers in the synapse triggers the dimer formation and the downstream events, even though we cannot exclude that post-translational modifications or interacting proteins could affect this pathway. Of note, the induction of LTD does not affect CAP2 localization in the spine and dimer formation, highlighting the specificity of this mechanism for LTP. Further experiments are required in *ex vivo* systems stimulating specific synaptic afferents, in order to assess input specificity of LTP induction that cannot be evaluated using a global chemical stimulation of the synapses.

Cofilin has been implicated in the pathophysiology of Alzheimer's disease, since cofilin accumulates in neurites close to senile plaques in Alzheimer's disease tissue and Alzheimer's disease mouse models (Bamburg and Bernstein, 2016). However, the mechanisms by which cofilin contributes to Alzheimer's disease pathogenesis remain quite controversial, as either an excessive activation (Kim *et al.*, 2013) or inactivation (Barone *et al.*, 2014; Rush *et al.*, 2018) have been reported in Alzheimer's disease patients. Here, we changed perspective, and bring into focus cofilin localization in spines in Alzheimer's disease, because it is directly regulated by LTP, as well as its association with CAP2 (Bosch *et al.*, 2014). The CAP2 dimer-dependent mechanism that regulates cofilin availability at the synapse is specifically affected in the hippocampus, but not in the SFG, of both Alzheimer's disease patients and APP/PS1 mice. Remarkably, we detected a significant increase in the CSF CAP2 levels in Alzheimer's disease patients but not in frontotemporal dementia patients, indicating the specificity of the alteration for this form of dementia. Accurate early and differential diagnosis across different forms of dementia represents a clinical challenge due to the complexity of neurodegenerative processes and is crucial for establishing prognosis and accessing adequate treatment (Palop *et al.*, 2006; Oxtoby *et al.*, 2017). Our preliminary study could set the stage for further studies aimed at confirming CAP2 as a potential biomarker of hippocampal synaptic dysfunction in Alzheimer's disease.

In the hippocampal synapses of Alzheimer's disease patients and Alzheimer's disease mouse model, we measured a dramatic increase in cofilin levels, along with a reduction in CAP2 synaptic availability, and accordingly a decrease in CAP2 dimer formation at the synapse.

Furthermore, we noticed that in Alzheimer's disease patients' hippocampi cofilin precipitates a different pattern of CAP2 monomeric and dimeric forms, suggesting the presence of an ineffective CAP2/cofilin complex in Alzheimer's disease hippocampal synapses that could contribute to the loss of structural plasticity of spines in Alzheimer's disease.

In the current paper, we explored the use of mixed-effects models to fully account for the complex design of multi-level hierarchically structured imaging data (Paternoster *et al.*, 2018); this approach improved our ability to control variability at culture and neuron levels and provided us more precise mean estimates (Lazic, 2010).

Together, our findings describe a novel CAP2-dependent mechanism controlling cofilin synaptic availability and actin turnover, which is closely interdependent to LTP. Furthermore, we show that the main players of this pathway are altered in Alzheimer's disease, adding new pieces to the puzzle in the understanding of the complex and coordinated events leading to early synaptic dysfunction and plasticity alterations in Alzheimer's disease pathogenesis.

Supplementary material

Supplementary material is available at *Brain Communications* online.

Acknowledgements

We thank A. Longhi and E. Zianni for technical assistance and Alessia Mariani, Filippo La Greca, Ramona Stringhi, and Michael Wolf for excellent practical work, Chiara Macchi and Massimiliano Ruscica for advice on ELISA assays. We thank UMIF (UKE, Hamburg) for access to their stimulated emission depletion imaging system. Part of this work was carried out at NOLIMITS, an advanced imaging facility established by the Università degli Studi di Milano. The brain tissues were obtained from the Netherlands Brain Bank, Netherlands Institute for Neuroscience, Amsterdam.

Funding

This project has received funding from the European Union's Horizon 2020 research and innovation program under the Marie Skłodowska-Curie grant agreement No 676144 (Synaptic Dysfunction in Alzheimer Disease, SyDAD) to M.D.L., from the Italian Ministry of Education, University and Research (MIUR) (PRIN 2015N4FKJ4 to M.D.L., PRIN 2017B9NCSX to E.M., Fondo per il Finanziamento delle Attività Base di Ricerca FFABR18_10 to E.M., MIUR Progetto Eccellenza), from Fondazione Cariplo to E.M. (Grant no. 2018—0511), from AIRAlzh Onlus-COOP Italia (fellowship to S.P.), from Boehringer Ingelheim Fonds (travel grant to S.P.), from an intramural grant of University of

Milan to E.M. (Fondo di sviluppo unimi- linea2—PSR2015-1716GRACA02_05_M and PSR2017_DIP_022_03 and PSR2019_EMARC) and to V.E. (PSR2015-1719FBRAV), from the Deutsche Forschungsgemeinschaft (DFG) [Emmy-Noether Programm (MI 1923/1-1) and FOR2419 (MI 1923/2-1 and MI 1923/2-2)] to M.M. and from DFG (SFB1158, project A08) to D.M. This work was supported by MIUR - PON ‘Ricerca e Innovazione’ PerMedNet project (ARS01_01226).

Competing interests

The authors report no competing interests.

References

- Andrianantoandro E, Pollard TD. Mechanism of actin filament turnover by severing and nucleation at different concentrations of ADF/cofilin. *Mol Cell* 2006; 24: 13–23.
- Balcer HI, Goodman AL, Rodal AA, Smith E, Kugler J, Heuser JE, et al. Coordinated regulation of actin filament turnover by a high-molecular-weight Srv2/CAP complex, cofilin, profilin, and Aip1. *Curr Biol* 2003; 13: 2159–69.
- Bamburg JR, Bernstein BW. Actin dynamics and cofilin-actin rods in Alzheimer disease. *Cytoskeleton (Hoboken)* 2016; 73: 477–97.
- Barone E, Mosser S, Fraering PC. Inactivation of brain cofilin-1 by age, Alzheimer’s disease and γ -secretase. *Biochim Biophys Acta* 2014; 1842: 2500–9.
- Bates D, Mächler M, Bolker B, Walker S. Fitting linear mixed-effects models using lme4. *J Stat Soft* 2015; 67: 1–48.
- Benjamini Y, Hochberg Y. Controlling the false discovery rate: a practical and powerful approach to multiple testing. *J R Stat Soc B* 1995; 57: 289–300.
- Bernstein BW, Bamburg JR. ADF/cofilin: a functional node in cell biology. *Trends Cell Biol* 2010; 20: 187–95.
- Bertling E, Hotulainen P, Mattila PK, Matilainen T, Salminen M, Lappalainen P. Cyclase-associated protein 1 (CAP1) promotes cofilin-induced actin dynamics in mammalian nonmuscle cells. *Mol Biol Cell* 2004; 15: 2324–34.
- Blalock EM, Geddes JW, Chen KC, Porter NM, Markesbery WR, Landfield PW. Incipient Alzheimer’s disease: microarray correlation analyses reveal major transcriptional and tumor suppressor responses. *Proc Natl Acad Sci USA* 2004; 101: 2173–8.
- Blanchoin L, Pollard TD. Mechanism of interaction of Acanthamoeba actophorin (ADF/Cofilin) with actin filaments. *J Biol Chem* 1999; 274: 15538–46.
- Bosch M, Castro J, Saneyoshi T, Matsuno H, Sur M, Hayashi Y. Structural and molecular remodeling of dendritic spine substructures during long-term potentiation. *Neuron* 2014; 82: 444–59.
- Bourne JN, Harris KM. Balancing structure and function at hippocampal dendritic spines. *Annu Rev Neurosci* 2008; 31: 47–67.
- Braak H, Braak E. Neuropathological stageing of Alzheimer-related changes. *Acta Neuropathol* 1991; 82: 239–59.
- Chaudhry F, Breitsprecher D, Little K, Sharov G, Sokolova O, Goode BL. Srv2/cyclase-associated protein forms hexameric shurikens that directly catalyze actin filament severing by cofilin. *Mol Biol Cell* 2013; 24: 31–41.
- Chen LY, Rex CS, Casale MS, Gall CM, Lynch G. Changes in synaptic morphology accompany actin signaling during LTP. *J Neurosci* 2007; 27: 5363–72.
- Cingolani LA, Goda Y. Actin in action: the interplay between the actin cytoskeleton and synaptic efficacy. *Nat Rev Neurosci* 2008; 9: 344–56.
- de Pins B, Cifuentes-Díaz C, Farah AT, López-Molina L, Montalban E, Sancho-Balsells A, et al. Conditional BDNF delivery from astrocytes rescues memory deficits, spine density, and synaptic properties in the 5xFAD mouse model of Alzheimer disease. *J Neurosci* 2019; 39: 2441–58.
- Dinamarca MC, Guzzetti F, Karpova A, Lim D, Mitro N, Musardo S, et al. Ring finger protein 10 is a novel synaptonuclear messenger encoding activation of NMDA receptors in hippocampus. *Elife* 2016; 5: e12430.
- Field J, Ye DZ, Shinde M, Liu F, Schillinger KJ, Lu M, et al. CAP2 in cardiac conduction, sudden cardiac death and eye development. *Sci Rep* 2015; 5: 17256.
- Frisoni GB, Fox NC, Jack CR, Scheltens P, Thompson PM. The clinical use of structural MRI in Alzheimer disease. *Nat Rev Neurol* 2010; 6: 67–77.
- Fukazawa Y, Saitoh Y, Ozawa F, Ohta Y, Mizuno K, Inokuchi K. Hippocampal LTP is accompanied by enhanced F-actin content within the dendritic spine that is essential for late LTP maintenance in vivo. *Neuron* 2003; 38: 447–60.
- Gardoni F, Bellone C, Cattabeni F, Di Luca M. Protein kinase C activation modulates alpha-calmodulin kinase II binding to NR2A subunit of N-methyl-D-aspartate receptor complex. *J Biol Chem* 2001; 276: 7609–13.
- Gu J, Lee CW, Fan Y, Komlos D, Tang X, Sun C, et al. ADF/cofilin-mediated actin dynamics regulate AMPA receptor trafficking during synaptic plasticity. *Nat Neurosci* 2010; 13: 1208–15.
- Henriques AG, Oliveira JM, Carvalho LP, da CE, Silva O. β influences cytoskeletal signaling cascades with consequences to Alzheimer’s disease. *Mol Neurobiol* 2015; 52: 1391–407.
- Hild G, Kalmár L, Kardos R, Nyitrai M, Bugyi B. The other side of the coin: functional and structural versatility of ADF/cofilins. *Eur J Cell Biol* 2014; 93: 238–51.
- Holtmaat A, Svoboda K. Experience-dependent structural synaptic plasticity in the mammalian brain. *Nat Rev Neurosci* 2009; 10: 647–58.
- Horch HW, Katz LC. BDNF release from single cells elicits local dendritic growth in nearby neurons. *Nat Neurosci* 2002; 5: 1177–84.
- Hotulainen P, Hoogenraad CC. Actin in dendritic spines: connecting dynamics to function. *J Cell Biol* 2010; 189: 619–29.
- Hotulainen P, Llano O, Smirnov S, Tanhuanpää K, Faix J, Rivera C, et al. Defining mechanisms of actin polymerization and depolymerization during dendritic spine morphogenesis. *J Cell Biol* 2009; 185: 323–39.
- Hubberstey AV, Mottillo EP. Cyclase-associated proteins: CAPacity for linking signal transduction and actin polymerization. *FASEB J* 2002; 16: 487–99.
- Jankowsky JL, Fadale DJ, Anderson J, Xu GM, Gonzales V, Jenkins NA, et al. Mutant presenilins specifically elevate the levels of the 42 residue beta-amyloid peptide in vivo: evidence for augmentation of a 42-specific gamma secretase. *Hum Mol Genet* 2004; 13: 159–70.
- Kaminari A, Giannakas N, Tzinia A, Tsilibary EC. Overexpression of matrix metalloproteinase-9 (MMP-9) rescues insulin-mediated impairment in the 5XFAD model of Alzheimer’s disease. *Sci Rep* 2017; 7: 683.
- Kasai H, Fukuda M, Watanabe S, Hayashi-Takagi A, Noguchi J. Structural dynamics of dendritic spines in memory and cognition. *Trends Neurosci* 2010; 33: 121–9.
- Kim T, Vidal GS, Djuricic M, William CM, Birnbaum ME, Garcia KC, et al. Human LILRB2 is a β -amyloid receptor and its murine homolog PirB regulates synaptic plasticity in an Alzheimer’s model. *Science* 2013; 341: 1399–404.
- Korobova F, Svitkina T. Molecular architecture of synaptic actin cytoskeleton in hippocampal neurons reveals a mechanism of dendritic spine morphogenesis. *Mol Biol Cell* 2010; 21: 165–76.
- Kotila T, Wioland H, Enkavi G, Kogan K, Vattulainen I, Jégou A, et al. Mechanism of synergistic actin filament pointed end depolymerization by cyclase-associated protein and cofilin. *Nat Commun* 2019; 10: 5320.

- Kumar A, Paeger L, Kosmas K, Kloppenburg P, Noegel AA, Peche VS. Neuronal actin dynamics, spine density and neuronal dendritic complexity are regulated by CAP2. *Front Cell Neurosci* 2016; 10: 180.
- Kuznetsova A, Brockhoff PB, Christensen R. lmerTest package: tests in linear mixed effects models. *J Stat Soft* 2017; 82: 1–26.
- Lazic SE. The problem of pseudoreplication in neuroscientific studies: is it affecting your analysis?. *BMC Neurosci* 2010; 11: 5.
- Lenth R. emmeans: Estimated Marginal Means, aka Least-Squares Means. R package version 1.4.5, 2020. Available from: <https://CRAN.R-project.org/package=emmeans> (20 April 2020, date last accessed).
- Liu Y, Xiao W, Shinde M, Field J, Templeton DM. Cadmium favors F-actin depolymerization in rat renal mesangial cells by site-specific, disulfide-based dimerization of the CAP1 protein. *Arch Toxicol* 2018; 92: 1049–64.
- Lynch G, Rex CS, Chen LY, Gall CM. The substrates of memory: defects, treatments, and enhancement. *Eur J Pharmacol* 2008; 585: 2–13.
- Malinverno M, Carta M, Epis R, Marcello E, Verpelli C, Cattabeni F, et al. Synaptic localization and activity of ADAM10 regulate excitatory synapses through N-cadherin cleavage. *J Neurosci* 2010; 30: 16343–55.
- Marcello E, Gardoni F, Luca Pérez-Otaño DM. I. An arginine stretch limits ADAM10 exit from the endoplasmic reticulum. *J Biol Chem* 2010; 285: 10376–84.
- Marcello E, Saraceno C, Musardo S, Vara H, la Fuente de AG, Pelucchi S, et al. Endocytosis of synaptic ADAM10 in neuronal plasticity and Alzheimer's disease. *J Clin Invest* 2013; 123: 2523–38.
- Matus A. Growth of dendritic spines: a continuing story. *Curr Opin Neurobiol* 2005; 15: 67–72.
- Mauceri D, Freitag HE, Oliveira AMM, Bengtson CP, Bading H. Nuclear calcium-VEGFD signaling controls maintenance of dendrite arborization necessary for memory formation. *Neuron* 2011; 71: 117–30.
- Mikhaylova M, Bär J, van Bommel B, Schätzle P, Yuanxiang P, Raman R, et al. Caldendrin directly couples postsynaptic calcium signals to actin remodeling in dendritic spines. *Neuron* 2018; 97: 1110–25.e14.
- Minamide LS, Striegl AM, Boyle JA, Meberg PJ, Bamburg JR. Neurodegenerative stimuli induce persistent ADF/cofilin-actin rods that disrupt distal neurite function. *Nat Cell Biol* 2000; 2: 628–36.
- Noegel AA, Rivero F, Albrecht R, Janssen KP, Köhler J, Parent CA, et al. Assessing the role of the ASP56/CAP homologue of Dictyostelium discoideum and the requirements for subcellular localization. *J Cell Sci* 1999; 112: 3195–203.
- Normoyle KPM, Briehner WM. Cyclase-associated protein (CAP) acts directly on F-actin to accelerate cofilin-mediated actin severing across the range of physiological pH. *J Biol Chem* 2012; 287: 35722–32.
- Okamoto K-I, Nagai T, Miyawaki A, Hayashi Y. Rapid and persistent modulation of actin dynamics regulates postsynaptic reorganization underlying bidirectional plasticity. *Nat Neurosci* 2004; 7: 1104–12.
- Ono S. The role of cyclase-associated protein in regulating actin filament dynamics - more than a monomer-sequestration factor. *J Cell Sci* 2013; 126: 3249–58.
- Oxtoby NP, Alexander DC, Consortium E. Imaging plus X: multimodal models of neurodegenerative disease. *Curr Opin Neurol* 2017; 30: 371–9.
- Palop JJ, Chin J, Mucke L. A network dysfunction perspective on neurodegenerative diseases. *Nature* 2006; 443: 768–73.
- Paternoster V, Rajkumar AP, Nyengaard JR, Børglum AD, Grove J, Christensen JH. The importance of data structure in statistical analysis of dendritic spine morphology. *J Neurosci Methods* 2018; 296: 93–8.
- Peche V, Shekar S, Leichter M, Korte H, Schröder R, Schleicher M, et al. CAP2, cyclase-associated protein 2, is a dual compartment protein. *Cell Mol Life Sci* 2007; 64: 2702–15.
- Peche VS, Holak TA, Burgute BD, Kosmas K, Kale SP, Wunderlich FT, et al. Ablation of cyclase-associated protein 2 (CAP2) leads to cardiomyopathy. *Cell Mol Life Sci* 2013; 70: 527–43.
- Pelucchi S, Stringhi R, Marcello E. Dendritic spines in Alzheimer's disease: how the actin cytoskeleton contributes to synaptic failure. *Int J Mol Sci* 2020; 21: 908.
- Penzen P, Cahill ME, Jones KA, Vanleeuwen J-E, Woolfrey KM. Dendritic spine pathology in neuropsychiatric disorders. *Nat Neurosci* 2011; 14: 285–93.
- Penzen P, Vanleeuwen J-E. Impaired regulation of synaptic actin cytoskeleton in Alzheimer's disease. *Brain Res Rev* 2011; 67: 184–92.
- Pinheiro J, Bates D. Mixed-effects models in S and S-PLUS. New York: Springer-Verlag; 2006.
- Pontrello CG, Sun M-Y, Lin A, Fiacco TA, DeFea KA, Ethell IM. Cofilin under control of β -arrestin-2 in NMDA-dependent dendritic spine plasticity, long-term depression (LTD), and learning. *Proc Natl Acad Sci USA* 2012; 109: E442–51.
- Purde V, Busch F, Kudryashova E, Wysocki VH, Kudryashov DS. Oligomerization affects the ability of human cyclase-associated proteins 1 and 2 to promote actin severing by cofilins. *Int J Mol Sci* 2019; 20: 5647.
- Quintero-Monzon O, Jonasson EM, Bertling E, Talarico L, Chaudhry F, Sihvo M, et al. Reconstitution and dissection of the 600-kDa Srv2/CAP complex: roles for oligomerization and cofilin-actin binding in driving actin turnover. *J Biol Chem* 2009; 284: 10923–34.
- R Core Team. R: a language and environment for statistical computing. Vienna, Austria: R Foundation For Statistical Computing; 2019.
- Racz B, Weinberg RJ. Spatial organization of cofilin in dendritic spines. *Neuroscience* 2006; 138: 447–56.
- Rush T, Martinez-Hernandez J, Dollmeyer M, Frandemiche ML, Borel E, Boisseau S, et al. Synaptotoxicity in Alzheimer's disease involved a dysregulation of actin cytoskeleton dynamics through cofilin 1 phosphorylation. *J Neurosci* 2018; 38: 10349–61.
- Rust MB, Gurniak CB, Renner M, Vara H, Morando L, Görlich A, et al. Learning, AMPA receptor mobility and synaptic plasticity depend on n-cofilin-mediated actin dynamics. *Embo J* 2010; 29: 1889–902.
- Rust MB. ADF/cofilin: a crucial regulator of synapse physiology and behavior. *Cell Mol Life Sci* 2015a; 72: 3521–9.
- Rust MB. Novel functions for ADF/cofilin in excitatory synapses - lessons from gene-targeted mice. *Commun Integr Biol* 2015b; 8: e1114194.
- Sala C, Segal M. Dendritic spines: the locus of structural and functional plasticity. *Physiol Rev* 2014; 94: 141–88.
- Shekhar S, Chung J, Kondev J, Gelles J, Goode BL. Synergy between cyclase-associated protein and Cofilin accelerates actin filament depolymerization by two orders of magnitude. *Nat Commun* 2019; 10: 5319.
- Smith KR, Kopeikina KJ, Fawcett-Patel JM, Leaderbrand K, Gao R, Schürmann B, et al. Psychiatric risk factor ANK3/ankyrin-G nanodomains regulate the structure and function of glutamatergic synapses. *Neuron* 2014; 84: 399–415.
- Star EN, Kwiatkowski DJ, Murthy VN. Rapid turnover of actin in dendritic spines and its regulation by activity. *Nat Neurosci* 2002; 5: 239–46.
- Van Troys M, Huyck L, Leyman S, Dhaese S, Vandekerckhove J, Ampe C. Ins and outs of ADF/cofilin activity and regulation. *Eur J Cell Biol* 2008; 87: 649–67.
- Yusof AM, Hu N-J, Wlodawer A, Hofmann A. Structural evidence for variable oligomerization of the N-terminal domain of cyclase-associated protein (CAP). *Proteins* 2004; 58: 255–62.
- Yuste R, Bonhoeffer T. Morphological changes in dendritic spines associated with long-term synaptic plasticity. *Annu Rev Neurosci* 2001; 24: 1071–89.
- Zhou Q, Homma KJ, Poo M-M. Shrinkage of dendritic spines associated with long-term depression of hippocampal synapses. *Neuron* 2004; 44: 749–57.